Politecnico di Torino

Department of Applied Science and Technology

Master Degree in Physics of Complex Systems

Dynamical transition in inhomogeneous TASEP

Supervisors:
Alessandro Pelizzola
Marco Pretti

Candidate:
Andrea Demaria

ACADEMIC YEAR 2024-2025

Acknowledgments

I deeply thank Alessandro Pelizzola and Marco Pretti for their assistance in the development of this thesis project. My thanks also go to my friends in Turin, in particular to Amedeo and Gabriele for they support in every step of this beautiful hard trip. Thanks to Gabriele and Livio, great friends from high school, who have been always available for any type of tips and suggestions.

In these long 5 years, I can't help but thank my family for believing in me. Thank you mum and dad for all your efforts to make my dream come true. Thanks to my brother, Nicola, for all the moments spent together with no thought for studying where I saw the importance to have someone by your side. Thanks to my grandfather, Carlo, for teaching me, especially in these last two months, the very important essences of life: health and love. Thanks to my grandmother, Silvana, who left me too soon, but I'm sure she would be proud of me. Thanks to my uncles, Manuela and Beppe, for helping me overcome all the obstacles during years.

Thanks to all people who supported me in this journey, but now they are no even more part of my life. In particular, I would like to thank a person who will surely be reading this page that helped me to believe in my strengths and taught me that nothing is forever. However, you will have always a part in my heart that I can't delete.

Thanks to PoliTo, for the opportunity to become acquainted with many interesting phenomena in Physics with the help of very passionate Professors.

Last, but not least, thanks to myself. Especially in these last two months I thought that all the efforts done before were useless, but with the help of the previous mentioned people I arrived to cross the line. If I have to choose a sentence that has accompanied me during these years, probably is the following one

"The value of things is determined by the effort we make to obtain them"

and honestly, I think that this master degree has a big personal value.

Contents

Acronyms

DWT Domain Wall Theory.

FLE Finite Lattice Extrapolation.

HD High Density.

LD Low Density.

MC Maximal Current.

MFT Mean Field Theory.

OBC Open Boundary Conditions.

TASEP Totally Asymmetric Simple Exclusion Process.

TASEP - LK Totally Asymmetric Simple Exclusion Process with Langmuir Kinetics.

Chapter 1

Introduction

Inspired by the huge relevance of simple exclusion processes models as biological traffic models or vehicular traffic as well, we will focus our work on the *Totally Asymmetric Simple Exclusion Process (TASEP)*.

The latter is defined on a one dimensional lattice, where each site could be occupied or not by only one particle. The particles can hop from left to right with a given hopping rate provided that the lattice site on the right is empty[1]. There is moreover a specified entry rate in the first lattice site where particles can enter in the system and exit rate from the last one where particles can exit the system. This is a sort of a skeleton of the model that can be filled with particular choices of rates at which hopping processes happen together with suitable boundary conditions. We consider the TASEP with *Open Boundary Conditions (OBC)* and non uniform, slowly varying, hopping rates with non zero entry rate only at the first site and non zero exit rate only from the last one. In a more general model, one could also consider non zero entry rates and non zero exit rates through all lattice sites giving rise to a generalization of the model called *Totally Asymmetric Simple Exclusion Process with Langmuir Kinetics (TASEP - LK)*. However, we do not focus on this version explicitly, but we make only some comments about it that will be clearly specified at the proper time.

The purpose of the present thesis is to investigate the so called dynamical transition making use of several analytical and numerical methods such as *Mean Field Theory (MFT), Domain Wall Theory (DWT)* and *Finite Lattice Extrapolation (FLE)*.

[1]We can therefore easily see the connection with traffic models. In particular, in biological contexts, the model is useful to describe the protein synthesis on mRNA via polyribosome; instead, in vehicular traffic, the model could describe cars moving forward on a one lane road.

Chapter 2

The model

In this chapter we analyse in detail the non homogeneous TASEP model with OBC. After a brief explanation of the needed variables and parameters, we will move to the description of the main phases the system face out through the phase diagram. Finally, we will discuss the stationarity behaviour of the model. All the results here presented are already known, however it is useful to describe it in order to become familiar with concepts and notations.

2.1 Definitions of variables and parameters

The TASEP model with OBC is defined on a one dimensional lattice of L sites each one labelled from left to right as

$$i = 1, \dots, L \tag{2.1}$$

with an occupation number random variable

$$n_i(t) = \begin{cases} 0, & \text{node } i \text{ not occupied at time } t \\ 1, & \text{node } i \text{ occupied at time } t \end{cases} \tag{2.2}$$

Particles can be injected in the system at the first lattice site $i = 1$ (provided it is empty with $n_1(t) = 0$) with rate $\alpha \in [0, 1]$ and can be extracted from the last lattice site $i = L$ (provided it is occupied with $n_L(t) = 1$) with rate $\beta \in [0, 1]$. Moreover, particles can hop from site i (provided it is occupied with $n_i(t) = 1$) to

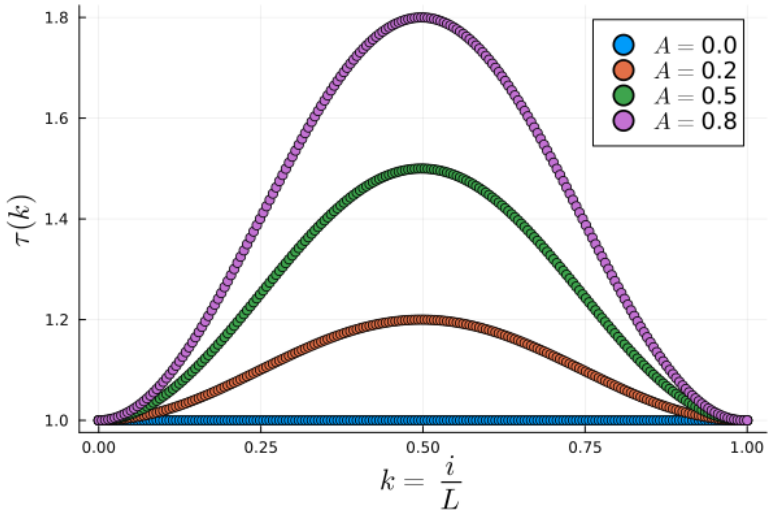

Figure 2.1: *Inverse of the hopping rates (mean hopping time)* $\tau(k)$ *as function of the scaled position variable* $\frac{i}{L}$ *with* $L = 200$ *at different values of* A.

$i + 1$ (provided it is empty with $n_{i+1}(t) = 0$) with hopping rate q_i. In the special inhomogeneous TASEP considered here, the hopping rates from one site to the adjacent one are characterized by a smooth spatial modulation according to the following function of the lattice site i

$$q_i = \left[1 + A \sin^2\left(\pi \frac{i}{L}\right)\right]^{-1}, \qquad i = 0, \ldots, L \tag{2.3}$$

where the constant $A \geq 0$ controls the minimum of the hopping rate function. This form of the hopping rates admit also a value for $i = 0$ and $i = L$ that in principle it is already included in the two boundary rates α and β. However, we can safely consider q_i as written before since $q_0 = q_L = 1$ in such a way that do not affect α and β. Sometimes it will be useful to regard q as a function of the scaled position variable $k = \frac{i}{L} \in [0, 1]$. In order to be clear, let us plot the profile that we have chosen. In particular in Figure 2.1 we report the profile of the mean hopping time $\tau(k) = q^{-1}(k)$. We can notice the existence of a unique maximum (unique minimum in q) and a flat behaviour constantly equal to 1 when $A = 0$ (uniform hopping rates).

A graphical representation of the entire model and its elementary kinetic processes on the lattice with L sites is reported in Figure 2.2 We can clearly see the particle - hole symmetry (a hole is equivalent to an empty site) which plays a crucial role in the different phases the system can face as explained in the following sections. It will be useful to define the average occupation in terms of local

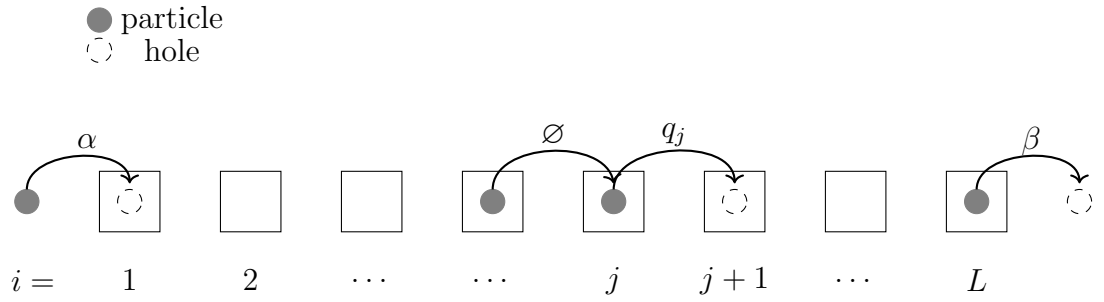

Figure 2.2: *TASEP scheme in OBC with injection rate α, extraction rate β and non homogeneous hopping rates q_j.*

densities at each lattice site i at time t

$$\rho_i(t) = \Big\langle n_i(t) \Big\rangle = \tag{2.4a}$$

$$= \mathbb{P}\Big(n_i(t) = 1\Big), \qquad i = 1, \dots, L \tag{2.4b}$$

where $\langle \cdot \rangle$ denotes the out of equilibrium average with respect to the realizations of the process. The average is clearly out of equilibrium since a current exists. Defining $J_i(t)$ the current from site i to $i+1$ at time t, we can interpret it as a joint probability that at time t the site i is occupied and the site $i+1$ is empty (hence a hopping transition can happen with rate q_i)

$$J_i(t) = q_i \mathbb{P}\Big(n_i(t) = 1, n_{i+1}(t) = 0\Big) \tag{2.5}$$

and performing MFT[2] for joint probability factorization in marginals, we arrive to

$$J_i(t) = q_i \mathbb{P}\Big(n_i(t) = 1\Big)\mathbb{P}\Big(n_{i+1}(t) = 0\Big) = \tag{2.7a}$$

$$= q_i \rho_i(t)\Big(1 - \rho_{i+1}(t)\Big), \qquad i = 1, \dots, L-1 \tag{2.7b}$$

[2]The mean field approximation assumes that at each time t the joint probability distribution factors into single node marginals (here denoted as $p_i\Big(n_i(t)\Big)$, hence both time and position dependent)

$$\mathbb{P}\Big(n_1(t), n_2(t), \dots, n_L(t)\Big) = \prod_{i=1}^{L} p_i\Big(n_i(t)\Big) \tag{2.6}$$

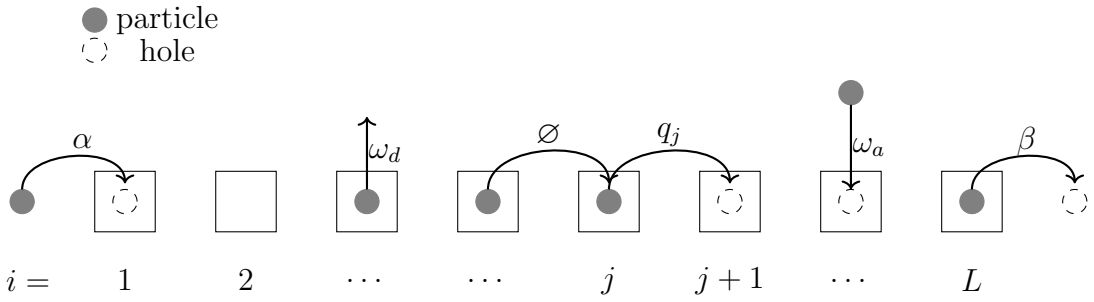

Figure 2.3: *TASEP - LK scheme in OBC with injection rate α, extraction rate β, non homogeneous hopping rates q_j, attachment rate ω_a and detachment rate ω_d independent on the sites.*

In the same way, we can define the two boundary currents to be proportional to the injection rate α and extraction rate β

$$J_0(t) = \alpha\Big(1 - \rho_1(t)\Big), \qquad J_L(t) = \beta\rho_L(t) \tag{2.8}$$

In order to be more uniform and clear we can write the current density as

$$J_i(t) = q_i\rho_i(t)\Big(1 - \rho_{i+1}(t)\Big), \qquad i = 0, \dots, L \tag{2.9}$$

where we have defined two boundary extra densities

$$\rho_0 = \alpha, \qquad \rho_{L+1} = 1 - \beta \tag{2.10}$$

assuming that the system is in contact with two reservoirs of fixed densities ρ_0, ρ_{L+1}.

Sometimes, as said previously, we will make use of the TASEP - LK model (see Botto et al. (2020)) whose schematic representation is reported in Figure 2.3 where bulk attachment and detachment processes occur at a large number of sites compared with the injection and extraction processes at the ends of the system.

Following Botto et al. (2018), local densities $\rho_i(t)$ have to obey a set of continuity equations. Taking into account the more general TASEP - LK model, we can write the variation in time of the local density in a specific site n as

$$\dot{\rho}_i(t) = J_{i-1}(t) - J_i(t) + \omega_a\Big(1 - \rho_i(t)\Big) - \omega_d\rho_i(t), \qquad i = 1, \dots, L \tag{2.11}$$

meaning that the positive contributions come from the current arriving from site $i-1$ or a particle attachment provided that the site i is empty; the negative contributions instead come from the current leaving site i or a particle detachment

provided that the site i is occupied. In the following we will make use of a shorthand notation $\chi' = 1 - \chi$, which permits us to write the expression of the density current (2.9) in MFT as

$$J_i(t) = q_i \rho_i(t) \rho_i'(t), \qquad i = 0. \ldots, L \tag{2.12}$$

with the usual boundary densities (2.10).

2.2 Phase diagram

Varying rates α and β, one can observe different behaviours of the system. In particular, there are three main phases

- *Low Density (LD)* phase characterized by

$$\alpha < \frac{1}{2}, \qquad \alpha < \beta \tag{2.13}$$

  where particles leave faster than they enter, with bulk density lower than $\frac{1}{2}$.

- *High Density (HD)* phase characterized by

$$\beta < \frac{1}{2}, \qquad \beta < \alpha \tag{2.14}$$

  where particles enter faster than they leave, with bulk density greater than $\frac{1}{2}$.

- *Maximal Current (MC)* phase characterized by

$$\alpha > \frac{1}{2}, \qquad \beta > \frac{1}{2} \tag{2.15}$$

  where the current acquires the maximum value.

The bulk of the system is intended as the entire system without the so called boundary layer at the left or at the right. The boundary layer is that region in which the stationary density does not follow the profile of the bulk one becoming a little bit higher or lower. However, in the analysis of the stationary densities we can really appreciate the difference.

According to Goswami et al. (2022) we can write, at steady state, due to the small variation of ρ_i from site i to $i + 1$

$$J = q(x)\rho(x)\Big(1 - \rho(x)\Big), \qquad x = \frac{i}{L} \tag{2.16}$$

where J is constant. Note that, since $q(x)$ has an explicit dependence on x, one should expect that also $\rho(x)$ is x dependent. Moreover, for a given fixed J one can retrieve two non uniform solutions $\rho_{\pm}(x)$

$$\rho_{\pm}(x) = \frac{1}{2}\left(1 \pm \sqrt{1 - \frac{4J}{q(x)}}\right) \tag{2.17}$$

where, since we want $\rho(x)$ to be real everywhere, an upper bound for the current arises

$$J \leq \frac{q(x)}{4} \implies J_{\max} = \frac{q_{\min}}{4} \tag{2.18}$$

Starting from the LD phase we can notice that the current in the bulk of the TASEP is equal to the entry one dictated by α, namely

$$J_{\text{LD}} = q(0)\alpha(1-\alpha) \tag{2.19}$$

with the constraint that $J_{\text{LD}} < J_{\max}$. Since the steady state bulk density is less than $\frac{1}{2}$ everywhere in this phase, the profile in the LD phase is given by

$$\rho_{\text{LD}}(x) = \frac{1}{2}\left(1 - \sqrt{1 - \frac{4J_{\text{LD}}}{q(x)}}\right) = \tag{2.20a}$$

$$= \frac{1}{2}\left(1 - \sqrt{1 - 4\frac{q(0)}{q(x)}\alpha(1-\alpha)}\right) \tag{2.20b}$$

where in our case $q(0) = 1$ and therefore could be omitted.

In the HD phase instead, we can notice that the density current in the bulk of the TASEP is equal to the exit one dictated by β, namely

$$J_{\text{HD}} = q(1)\beta(1-\beta) \tag{2.21}$$

with the constraint that $J_{\text{HD}} < J_{\max}$. Since the steady state bulk density is greater than $\frac{1}{2}$ everywhere in this phase, the profile in the HD phase is given by

$$\rho_{\text{HD}}(x) = \frac{1}{2}\left(1 + \sqrt{1 - \frac{4J_{\text{HD}}}{q(x)}}\right) = \tag{2.22a}$$

$$= \frac{1}{2}\left(1 + \sqrt{1 - 4\frac{q(1)}{q(x)}\beta(1-\beta)}\right) \tag{2.22b}$$

where in our case $q(1) = 1$ and therefore could be omitted.

Finally, in the MC phase, the density current exhibits its maximum value

$$J_{\mathrm{MC}} = \frac{q_{\min}}{4} \tag{2.23}$$

and the corresponding density profile is a combination of both $\rho_{\pm}(x)$ whose intersection is at the point x_0 such that

$$q(x_0) = q_{\min} \tag{2.24}$$

where the value reached is $\frac{1}{2}$.

How can these three phases be represented on a plane α/β? We need to determine the boundaries at which the phases meet.

Following again Goswami et al. (2022), the boundary between the LD and HD phases is dictated by the fact that the two respective bulk currents (2.19) and (2.21) are equal. From that condition it follows that

$$\alpha(1-\alpha) = \beta(1-\beta) \tag{2.25}$$

which is verified for $\alpha = \beta$ or $\alpha = 1 - \beta$. Since $\beta < \frac{1}{2}$ in the HD phase and $\alpha < \frac{1}{2}$ in the LD phase, $\alpha = \beta$ gives the LD - HD phase boundary. It reduces to the well known result for the coexistence line in a TASEP with uniform hopping rate function $q(x) \equiv 1$. Indeed, this is a consequence of the fact that we have ensured $q(0) = q(1)$ in such a way that (2.25) can be written in that form.

The boundary between the LD and MC phases instead is computed by imposing the equality between the two respective bulk currents (2.19) and (2.23). From that condition it follows that

$$\alpha_{\mathrm{LD/MC}} = \frac{1}{2}\left(1 - \sqrt{1 - \frac{q_{\min}}{q(0)}}\right) \tag{2.26}$$

is the boundary since $\alpha < \frac{1}{2}$ in the LD phase.

In the end, the boundary between the HD and MC phases is obtained by imposing the equality between the two respective bulk currents (2.21) and (2.23). From that condition it follows that

$$\beta_{\mathrm{HD/MC}} = \frac{1}{2}\left(1 - \sqrt{1 - \frac{q_{\min}}{q(1)}}\right) \tag{2.27}$$

is the boundary since $\beta < \frac{1}{2}$ in the HD phase.

As we can notice, the last two boundaries depend on the minimum of the hopping rate function which in turn is a function of the parameter A. In particular, from (2.3) it follows

$$q_{\min} = \frac{1}{1+A} \tag{2.28}$$

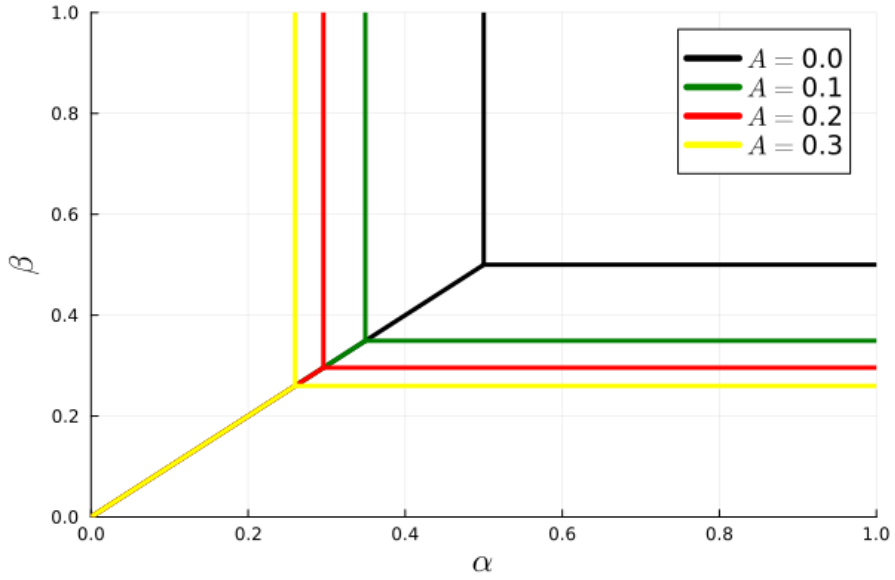

Figure 2.4: *Phase diagram of the TASEP model for different values of the constant* $A \geq 0$. *The HD region is bottom right, the LD region is top left and the MC region is top right.*

obtaining that the boundaries are exactly equal

$$\alpha_{\text{LD/MC}} = \beta_{\text{HD/MC}} = \frac{1}{2}\left(1 - \sqrt{\frac{A}{1+A}}\right) \tag{2.29}$$

due to the fact that $q(0) = q(1) = 1$. The expression of the boundaries always exists for $A \geq 0$. Note that the case $A = 0$ corresponds to the ordinary TASEP with uniform rates with the boundaries $\alpha_{\text{LD/MC}} = \beta_{\text{HD/MC}} = \frac{1}{2}$.

The phase diagram for different values of A is shown in Figure 2.4 where we can notice that by increasing the value of A, the MC region expands, as predicted by the boundaries (2.29).

2.3 Stationary density profiles

Looking at the stationary density profiles, the time dependence in (2.11) is not appearing anymore[3] and setting the time derivative equal to 0 together with (2.12)

[3]When we are looking for the stationary behaviour of a time dependent quantity $\gamma_i(t)$, we will drop the time dependence writing γ_i.

we arrive to

$$\rho_i \left(q_i \rho'_{i+1} + \omega_d \right) = \left(q_{i-1} \rho_{i-1} + \omega_a \right) \rho'_i, \qquad i = 1, \ldots, L \tag{2.30}$$

which can be solved numerically by recasting it into a fixed point form, namely

$$\rho_i = \left(1 + \frac{q_i \rho'_{i+1} + \omega_d}{q_{i-1} \rho_{i-1} + \omega_a} \right)^{-1}, \qquad i = 1, \ldots, L \tag{2.31}$$

while keeping fixed

$$\begin{cases} \rho_0 = \alpha \\ \rho_{L+1} = 1 - \beta \end{cases}, \quad \begin{cases} q_0 = 1 \\ q_L = 1 \end{cases} \tag{2.32}$$

Solving the recursive equation (2.31) with $\omega_d = \omega_a = 0$ numerically with a suitable initial condition (we have assumed an empty lattice except for the boundaries) we reached convergence and we have the entire profile of the stationary density. This profile is composed by a bulk region and a boundary layer region. The bulk region is the one that we have described before satisfying (2.20b) for the LD phase, (2.22b) for the HD phase and the constraint (2.24) for the MC phase. The boundary layer region instead is the one that deviates from the bulk region. In particular we can notice a right boundary layer in the LD phase, a left boundary layer in the HD phase and both left and right boundary layers in the MC phase. In Figure 2.5 the LD stationary density profiles for $A = 1$ and $A = 0$ are reported with a right boundary layer. The HD stationary density profiles for $A = 1$ and $A = 0$ are shown in Figure 2.6 with a left boundary layer. In these phases the current of the inhomogeneous model coincides with that of the homogeneous one and satisfies (2.18). Finally, in Figure 2.7 the MC stationary density profile for $A = 1$ and $A = 0$ is presented with both the right and the left boundary layer. As expected, here the two currents do not coincide because in the case of $A = 0$ the maximal current is $\frac{1}{4}$, whereas for $A \neq 0$ the maximal current is $\frac{q_{\min}}{4}$.

The main goal now is to investigate the relaxation process towards the stationary state through different methods that we have briefly mentioned in the introduction.

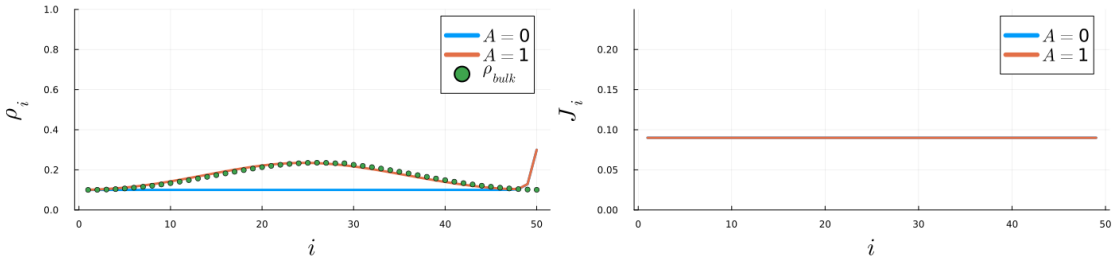

Figure 2.5: *LD stationary density profile (on the left) with uniform hopping rates (in blue) and non homogeneous ones (in orange) together with the bulk region* (2.20b) *for* $L = 50, \alpha = 0.1$ *and* $\beta = 0.3$. *On the right there is the density current in same conditions.*

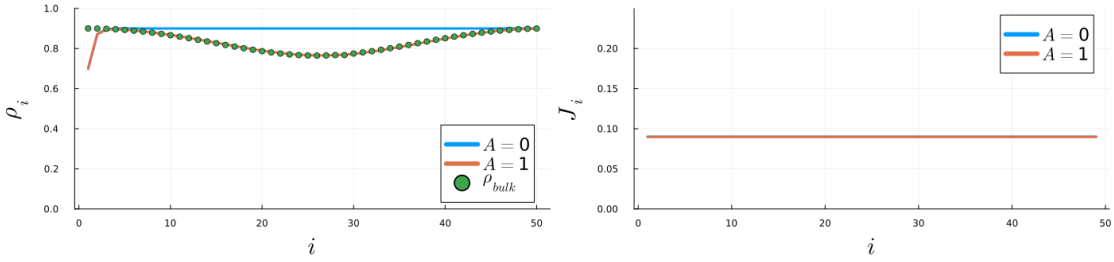

Figure 2.6: *HD stationary density profile (on the left) with uniform hopping rates (in blue) and non homogeneous ones (in orange) together with the bulk region* (2.22b) *for* $L = 50, \alpha = 0.3$ *and* $\beta = 0.1$. *On the right there is the density current in same conditions.*

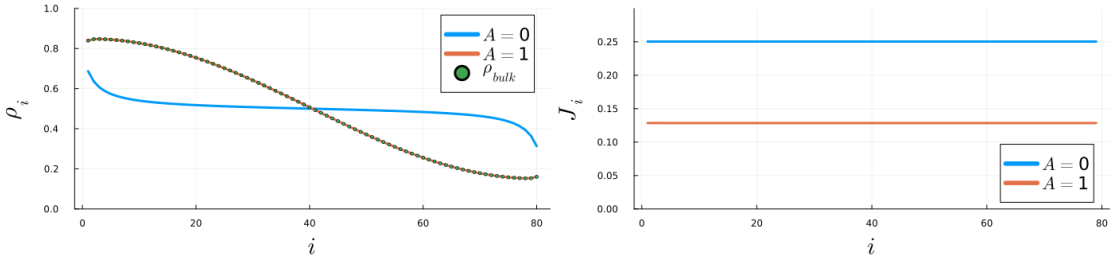

Figure 2.7: *MC stationary density profile (on the left) with uniform hopping rates (in blue) and non homogeneous ones (in orange) together with the constraint* (2.24) *due to the profiles in the bulk region for* $L = 80, \alpha = \beta = 0.8$.

Chapter 3

Relaxation to stationary state

We will analyse the relaxation to the stationary state with particular attention to the slowest relaxation rate, that is the inverse of the longest relaxation time. In the treatment we make use of the MFT, DWT and FLE.

3.1 Mean field theory

Taking inspiration from Pelizzola and Pretti (2017) we can linearize the mean field equations (2.11) for the time evolution of local densities around the stationary state solution

$$\dot{\rho}_i(t) = -\sum_{j=1}^{L} M_{i,j}\Big(\rho_j(t) - \rho_j\Big), \qquad i = 1, \dots, L \tag{3.1}$$

where the matrix $M \in \mathbb{R}^{L\times L}$ characterizes the relaxation. In particular, its smallest eigenvalue corresponds to the slowest relaxation rate.

Looking at (2.11) in the case of the TASEP model (set $\omega_a = \omega_d = 0$) the entries of M are non vanishing only over the diagonal, lower diagonal and upper diagonal.

Indeed

$$\begin{cases} M_{i,i} = -\frac{\partial \dot{\rho}_i(t)}{\partial \rho_i(t)}\Big|_{t\to+\infty}, & i = 1,\dots,L \\ M_{i,i-1} = -\frac{\partial \dot{\rho}_i(t)}{\partial \rho_{i-1}(t)}\Big|_{t\to+\infty}, & i = 2,\dots,L \\ M_{i,i+1} = -\frac{\partial \dot{\rho}_i(t)}{\partial \rho_{i+1}(t)}\Big|_{t\to+\infty}, & i = 1,\dots,L-1 \end{cases} \tag{3.2}$$

are the only non vanishing derivatives whose explicit result is

$$\begin{cases} M_{i,i} = q_i(1-\rho_{i+1}) + q_{i-1}\rho_{i-1}, & i = 1,\dots,L \\ M_{i,i-1} = -q_{i-1}(1-\rho_i), & i = 2,\dots,L \\ M_{i,i+1} = -q_i\rho_i, & i = 1,\dots,L-1 \end{cases} \tag{3.3}$$

resulting in a tridiagonal matrix. Unfortunately, the latter is not a Toeplitz[4] one as in the TASEP model with uniform hopping rates ($A = 0$) and $\alpha = 1-\beta$. This means that the minimum (non vanishing) eigenvalue has not an explicit analytical closed form and we have to proceed numerically. In particular, we are interested in the slowest relaxation rate in the infinite size limit $L \to +\infty$.

The computational evaluation of the eigenvalues is performed with the QR decomposition of the relaxation matrix whose detailed explanation can be found in Appendix A. The latter leads to complex eigenvalues, indeed the matrix in principle is not symmetric. We will see later that M can be symmetrized leading to zero imaginary part of eigenvalues. The spectrum for $A = 0.1$ in HD phase with suitable α and β is reported in Figure 3.1 where we can notice that the real part of the eigenvalues is dominant with respect to the imaginary part.

[4]A matrix $\Xi \in \mathbb{R}^{L\times L}$ acquires a Toeplitz form if each diagonal has a constant value

$$\Xi_{i,i+k} \equiv a_k, \qquad i = 1,\dots,L, \qquad k = 1-i,\dots,L-i \tag{3.4}$$

where $\{a_k\}_{k=-(L-1)}^{L-1} \in \mathbb{R}$. Indeed, in the case of uniform hopping rates ($A = 0$), the bulk stationary densities are uniform in all phases (see Figure 2.5, Figure 2.6 and Figure 2.7) leading to a Toeplitz relaxation matrix with $\alpha = 1-\beta$

$$a_0 = 1, \qquad a_1 = \beta - 1, \qquad a_{-1} = -\beta, \qquad a_j = 0, \quad \forall j = \pm 2, \pm 3, \dots, \pm(L-1) \tag{3.5}$$

whose minimum eigenvalue satisfies

$$\lambda_1 = 1 - 2\sqrt{\beta(1-\beta)}\cos\frac{\pi}{L+1} \overset{L\to+\infty}{\longrightarrow} 1 - 2\sqrt{\beta(1-\beta)} \tag{3.6}$$

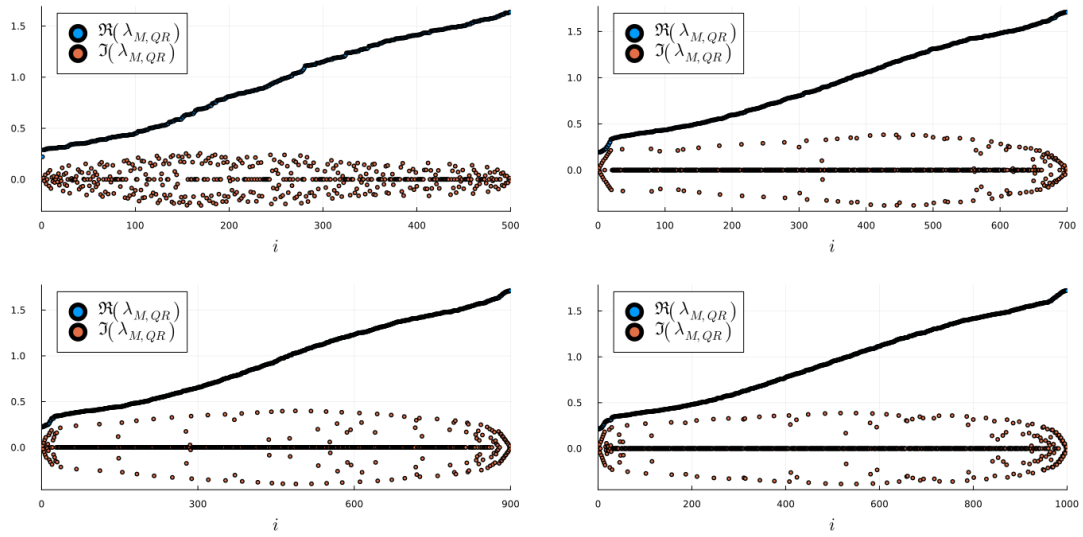

Figure 3.1: *Real and imaginary parts of the eigenvalues of M in HD phase computed with QR algorithm. The entry and exit rates are $\alpha = 0.1, \beta = 0.3$ and increasing size of the system $L = 500, 700, 900, 1000$.*

The imaginary parts of the eigenvalues are only a numerical effect that can be avoided by symmetrizing the matrix M. Following Botto et al. (2018) the eigenvalue problem associated with the relaxation matrix is

$$M_{i,i}v_i + M_{i,i+1}v_{i+1} + M_{i,i-1}v_{i-1} = \lambda v_i, \qquad i = 1, \dots, L \tag{3.7}$$

where λ is the eigenvalue and v_i are the eigenvectors components with $v_0 = v_{L+1} = 0$. The generic relaxation mode of the system

$$y_i(t) = v_i e^{-\lambda t}, \qquad i = 0, \dots, L+1 \tag{3.8}$$

in which $y_i(t)$ is a (small) time dependent perturbation of local densities with respect to the stationary ones

$$\rho_i(t) = \rho_i + y_i(t), \qquad i = 0, \dots, L+1 \tag{3.9}$$

Solving the eigenvalue problem (3.7) leads to complex eigenvalues in principle, however since the off diagonal entries of M never change sign it can be possible to perform a symmetrization of the matrix that we denote by M_{sym}. The latter is a simple similarity transformation which preserves the eigenvalues of the original matrix M.

In detail, one has to find an invertible matrix $P \in \mathbb{R}^{L \times L}$ such that

$$M_{\text{sym}} = P^{-1} M P \tag{3.10}$$

Choosing P to be diagonal

$$P = \mathbf{diag}(d_1, \dots, d_L) \tag{3.11}$$

we have to ensure

$$\left(P^{-1}MP\right)_{i,i+1} = \left(P^{-1}MP\right)_{i+1,i} \quad , \qquad i = 1, \dots, L-1 \tag{3.12}$$

which leads to the following condition on the entries of P

$$d_i = d_{i+1}\sqrt{\frac{\rho_i}{\rho'_{i+1}}}, \qquad i = 1, \dots, L-1 \tag{3.13}$$

Starting from $d_L = 1$ the entries of the invertible diagonal matrix P has to satisfy

$$\begin{cases} d_i = \prod_{k=i}^{L-1} \sqrt{\frac{\rho_k}{\rho'_{k+1}}}, & i = 1, \dots, L-1 \\ d_L = 1 \end{cases} \tag{3.14}$$

implying that the elements above and below the diagonal of M_{sym} coincide, indeed the upper diagonal has elements

$$\begin{aligned}
(M_{\text{sym}})_{i,i+1} &= \left(P^{-1}MP\right)_{i,i+1} = && \text{(3.15a)} \\
&= \frac{1}{d_i} M_{i,i+1} d_{i+1} = && \text{(3.15b)} \\
&= -\left(\prod_{k=i}^{L-1} \sqrt{\frac{\rho_k}{\rho'_{k+1}}}\right)^{-1} q_i \rho_i \prod_{k=i+1}^{L-1} \sqrt{\frac{\rho_k}{\rho'_{k+1}}} = && \text{(3.15c)} \\
&= -\left(\sqrt{\frac{\rho_i}{\rho'_{i+1}}}\right)^{-1} q_i \rho_i = && \text{(3.15d)} \\
&= -q_i \sqrt{\rho'_{i+1}\rho_i}, \qquad i = 1, \dots, L-1 && \text{(3.15e)}
\end{aligned}$$

whereas the lower diagonal, with a similar procedure, has elements

$$(M_{\text{sym}})_{i,i-1} = -q_{i-1}\sqrt{\rho_{i-1}\rho'_i}, \qquad i = 2, \dots, L \tag{3.16}$$

Furthermore, it can easily be seen that the diagonal elements are left unchanged leading to the eigenvalue problem

$$M_{i,i}u_i - q_i\sqrt{\rho_i\rho'_{i+1}}u_{i+1} - q_{i-1}\sqrt{\rho_{i-1}\rho'_i}u_{i-1} = \lambda u_i, \qquad i = 1, \dots, L \tag{3.17}$$

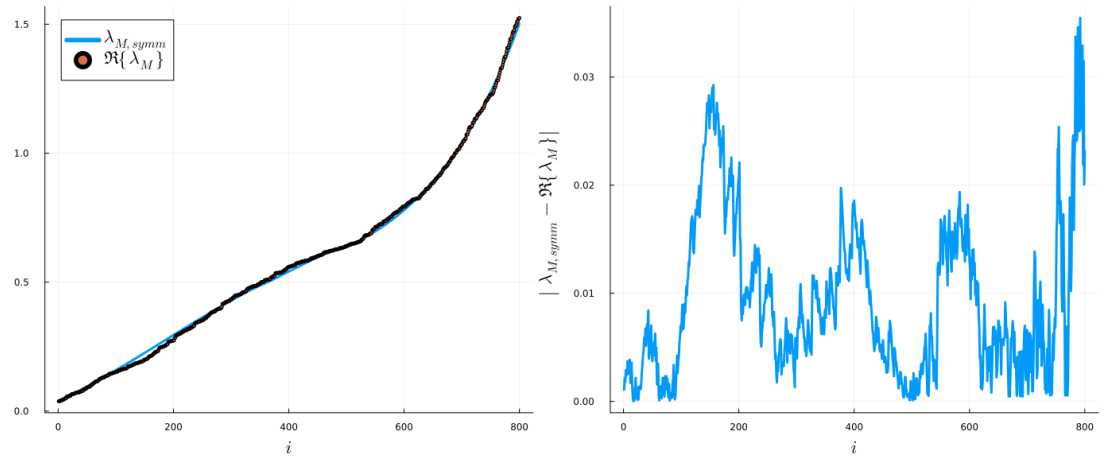

Figure 3.2: *Comparison between the spectrum of the symmetrized problem* (3.17) *with the real part of that of* (3.7) *in the HD phase with* $\alpha = 0.8, \beta = 0.07, A = 2, L = 800$. *On the left there is the entire spectrum, whereas on the right is shown the absolute difference between the two curves.*

where

$$u_i = v_i \prod_{k=0}^{i-1} \sqrt{\frac{\rho_k}{\rho'_{k+1}}}, \qquad i = 0, \dots, L+1 \tag{3.18}$$

with $u_0 = u_{L+1} = 0$. The spectrum of (3.17) is completely real and a good agreement is found with the real part of the spectrum of (3.7) as shown in Figure 3.2.

In order to find the slowest relaxation rate in the infinite size limit we can find suitable upper and lower bounds, which may coincide in the limit $L \to +\infty$. The following procedure is explained in detailed in Botto et al. (2020) for the case of TASEP - LK with uniform hopping rates. In the following we will generalize the same procedure in the presence of TASEP with non uniform hopping rates.

The equation (3.17) can be written by mapping the generic vector $u = (u_1, \dots, u_L)$ to $M_{\text{sym}}u$ whose components are

$$(M_{\text{sym}}u)_i = M_{i,i}u_i - q_i\sqrt{\tilde{J}_i}u_{i+1} - q_{i-1}\sqrt{\tilde{J}_{i-1}}u_{i-1}, \qquad i = 1, \dots, L \tag{3.19}$$

where

$$\tilde{J}_i = \rho_i \rho'_{i+1} \tag{3.20}$$

The slowest relaxation rate is the minimum eigenvalue of $M_{\text{sym}} \in \mathbb{R}^{L \times L}$ that we denote by $\lambda_{\text{min}}^{(L)}$. The goal is the analytical derivation of the asymptotic value $\lambda_{\text{min}}^{(\infty)}$

in the HD phase. Starting from (3.19) we will now determine the upper bounds in the thermodynamic limit, which may coincide with the actual value.

3.1.1 First upper bound

According to Courant's minimax principle

$$\lambda_{\min}^{(L)} \leq (u, M_{\text{sym}} u)\,, \qquad \forall u \in \mathbb{R}^L : \|u\| = 1 \tag{3.21}$$

where

$$(a, b) = \sum_{i=1}^{L} a_i b_i \tag{3.22}$$

is the standard scalar product. From now on we can always assume that u has unitary norm leading to (3.21) satisfied. The right hand side of the inequality can be explicitly written in our specific case as

$$(u, M_{\text{sym}} u) = \sum_{i=1}^{L} u_i \left(M_{\text{sym}} u\right)_i = \tag{3.23a}$$

$$= \sum_{i=1}^{L} u_i \left(M_{i,i} u_i - q_i \sqrt{\tilde{J}_i} u_{i+1} - q_{i-1} \sqrt{\tilde{J}_{i-1}} u_{i-1} \right) = \tag{3.23b}$$

$$= \sum_{i=1}^{L} M_{i,i} u_i^2 - \sum_{i=1}^{L} u_i q_i \sqrt{\tilde{J}_i} u_{i+1} - \sum_{i=1}^{L} u_i q_{i-1} \sqrt{\tilde{J}_{i-1}} u_{i-1} = \tag{3.23c}$$

$$= \sum_{i=1}^{L} M_{i,i} u_i^2 - 2 \sum_{i=1}^{L-1} u_i q_i \sqrt{\tilde{J}_i} u_{i+1} \tag{3.23d}$$

where the last line follows from $u_0 = u_{L+1} = 0$. Working a little bit on the diagonal $M_{i,i}$, we can make use of (2.22b) in the discretized version

$$\rho_i^{(\text{HD})} = \frac{1}{2} \left(1 + \sqrt{1 - 4 \frac{q_L}{q_i} \beta (1 - \beta)} \right) \tag{3.24}$$

to define the detrended densities r_i by subtracting from the local densities the non uniform part of the bulk profile

$$r_i = \rho_i - \left(\rho_i^{(\text{HD})} - \rho_0^{(\text{HD})} \right), \qquad i = 0, \ldots, L+1 \tag{3.25}$$

In this way, the diagonal $M_{i,i}$ results

$$M_{i,i} = q_i - q_i\rho_{i+1} + q_{i-1}\rho_{i-1} = \tag{3.26a}$$

$$= q_i - q_i\left(r_{i+1} + \rho_{i+1}^{(\mathrm{HD})} - \rho_0^{(\mathrm{HD})}\right) + q_{i-1}\left(r_{i-1} + \rho_{i-1}^{(\mathrm{HD})} - \rho_0^{(\mathrm{HD})}\right) = \tag{3.26b}$$

$$= q_i - (q_i r_{i+1} - q_{i-1}r_{i-1}) - \left(\rho_{i+1}^{(\mathrm{HD})}q_i - \rho_{i-1}^{(\mathrm{HD})}q_{i-1}\right) + \rho_0^{(\mathrm{HD})}(q_i - q_{i-1}) \simeq \tag{3.26c}$$

$$\simeq q_i - (q_i r_{i+1} - q_{i-1}r_{i-1}) \tag{3.26d}$$

where the last line follows from the sufficiently smooth behaviour of the hopping rates and of the bulk density profile. This leads us to write

$$(u, M_{\mathrm{sym}}u) \simeq \sum_{i=1}^{L} q_i u_i^2 - \sum_{i=1}^{L}(q_i r_{i+1} - q_{i-1}r_{i-1})u_i^2 - 2\sum_{i=1}^{L-1} u_i q_i \sqrt{\tilde{J}_i}u_{i+1} \tag{3.27}$$

For a given $C > 1$ we can define the sequence

$$y_i = \sqrt{\frac{2}{C}}\sin\left(\frac{\pi i}{C}\right) \tag{3.28}$$

for which the following properties are satisfied

$$\sum_{i=1}^{C-1} y_i^2 = 1, \qquad \sum_{i=1}^{C-2} y_i y_{i+1} = \cos\left(\frac{\pi}{C}\right) \tag{3.29}$$

In particular, the first one allows us to choose a normalize vector u as

$$u_i = \begin{cases} y_{i-m}, & i \in [m, m+C] \\ 0, & \text{otherwise} \end{cases}, \qquad i = 1, \dots, L \tag{3.30}$$

for any $C \in \{2, \dots, L+1\}$ where m denotes the site at which the minimum of the hopping rate is achieved

$$m = \arg\min_i q_i \tag{3.31}$$

At least numerically a posteriori, in the $L \to +\infty$ limit, the difference $r_{i+1} - r_{i-1}$ vanishes exponentially (see Botto et al. (2020) for the case of TASEP - LK) that together with the smooth hopping rate function lead to

$$\sum_{i=1}^{L}(q_i r_{i+1} - q_{i-1}r_{i-1})u_i^2 \simeq 0 \tag{3.32}$$

obtaining that

$$(u, M_{\text{sym}}u) \simeq \sum_{i=1}^{L} q_i u_i^2 - 2\sum_{i=1}^{L-1} u_i q_i \sqrt{\tilde{J}_i} u_{i+1} = \tag{3.33a}$$

$$= \sum_{i=m}^{m+C} q_i y_{i-m}^2 - 2\sum_{i=m}^{m+C} q_i \sqrt{\tilde{J}_i} y_{i-m} y_{i-m+1} \tag{3.33b}$$

where we take care of choosing C in such a way that for $L \to +\infty$ one has $C \to +\infty$. Due to (3.20) and the current in the HD phase (2.21)

$$\tilde{J}_i = \frac{\beta\beta'}{q_i} \tag{3.34}$$

implying

$$(u, M_{\text{sym}}u) = \sum_{i=m}^{m+C} q_i y_{i-m}^2 - 2\sqrt{\beta\beta'} \sum_{i=m}^{m+C} \sqrt{q_i} y_{i-m} y_{i-m+1} \tag{3.35}$$

Due to the smooth hopping rate function, in the interval $[m, m+C]$ with $C > 1$ finite we can approximate each q_i as $q_m = q_{\min}$

$$(u, M_{\text{sym}}u) \simeq q_{\min} \sum_{i=m}^{m+C} y_{i-m}^2 - 2\sqrt{q_{\min}\beta\beta'} \sum_{i=m}^{m+C} y_{i-m} y_{i-m+1} = \tag{3.36a}$$

$$= q_{\min} \sum_{n=0}^{C} y_n^2 - 2\sqrt{q_{\min}\beta\beta'} \sum_{n=0}^{C} y_n y_{n+1} = \tag{3.36b}$$

$$= q_{\min} \sum_{n=1}^{C-1} y_n^2 - 2\sqrt{q_{\min}\beta\beta'} \sum_{n=1}^{C-2} y_n y_{n+1} = \tag{3.36c}$$

$$= q_{\min} - 2\sqrt{q_{\min}\beta\beta'} \cos\left(\frac{\pi}{C}\right) \tag{3.36d}$$

where we used previous properties and the definition of y_i. Finally, taking the infinite size limit (which coincides with the $C \to +\infty$ limit), the inequality (3.21) acquire the following form

$$\lambda_{\min}^{(\infty)} \leq q_{\min} - 2\sqrt{q_{\min}\beta\beta'} \tag{3.37}$$

3.1.2 Second upper bound

Let us define the function

$$f(x) = \sum_{i=1}^{+\infty} \frac{s_{i+1} - s_{i-1}}{\sqrt{\beta\beta'}} v_i(x) \zeta^i(x) \tag{3.38}$$

where

$$\zeta(x) = x - \sqrt{x^2 - 1} \tag{3.39}$$

while the sequences s_i and $v_i(x)$ are defined in a recursive way as

$$\begin{cases} s_0 = \alpha \\ s_{i+1} = 1 - \frac{\beta\beta'}{s_i}, \qquad i = 0, 1, \dots L-1 \end{cases} \tag{3.40}$$

and

$$\begin{cases} v_0(x) = 0 \\ v_1(x) = 1 \\ v_{i+1}(x) = \Big(2x - 2x_0(s_{i+1} - s_{i-1})\Big)v_i(x) - v_{i-1}(x), \qquad i = 1, 2, \dots, L-1 \end{cases} \tag{3.41}$$

where

$$x_0 = \frac{1}{2\sqrt{\beta\beta'}} \tag{3.42}$$

Furthermore we denote by x_* the point at which the function f is unitary

$$f(x_*) = 1 \tag{3.43}$$

In order to obtain good bounds, the idea is that of choosing u as close as possible to the actual eigenvector

$$u_i = \frac{v_i(x_*)}{A_L(x_*)} \tag{3.44}$$

where $A_L(x_*)$ is a normalization factor

$$A_L(x_*) = \sqrt{\sum_{i=1}^{L} v_i^2(x_*)} \tag{3.45}$$

Rewriting the recursive definition for $v_i(x_*)$ in terms of u_n we obtain

$$u_{i+1}A_L(x_*) = \Big(2x_* - 2x_0(s_{i+1} - s_{i-1})\Big)u_i A_L(x_*) - u_{i-1}A_L(x_*) \tag{3.46}$$

which implies

$$2x_0(s_{i+1} - s_{i-1})u_i = 2x_* u_i - u_{i+1} - u_{i-1} \tag{3.47}$$

Multiplying both sides by u_i and summing over i (remembering that $u_0 = u_{L+1} = 0$) we obtain

$$2x_0 \sum_{i=1}^{L}(s_{i+1} - s_{i-1})u_i^2 = 2x_* \underbrace{\sum_{i=1}^{L} u_i^2}_{1} - \sum_{i=1}^{L} u_{i+1}u_i - \sum_{i=1}^{L} u_{i-1}u_i = \tag{3.48a}$$

$$= 2x_* - \left(\sum_{i=1}^{L-1} u_{i+1}u_i + \sum_{i=2}^{L} u_{i-1}u_i\right) = \tag{3.48b}$$

$$= 2x_* - 2\sum_{i=1}^{L-1} u_{i+1}u_i \tag{3.48c}$$

implying

$$\sum_{i=1}^{L}(s_{i+1} - s_{i-1})u_i^2 = \frac{x_*}{x_0} - \frac{1}{x_0}\sum_{i=1}^{L-1} u_{i+1}u_i \tag{3.49}$$

At least numerically a posteriori, the detrended densities tend to the sequence s_i for $L \to +\infty$, hence the scalar product (3.27) can be written as

$$(u, M_{\text{sym}}u) \simeq \sum_{i=1}^{L} q_i u_i^2 - \sum_{i=1}^{L}(q_i s_{i+1} - q_{i-1}s_{i-1})u_i^2 - 2\sum_{i=1}^{L-1} u_i q_i \sqrt{\tilde{J}_i} u_{i+1} \simeq \tag{3.50}$$

$$\simeq \sum_{i=1}^{L} q_i u_i^2 - \sum_{i=1}^{L} q_i(s_{i+1} - s_{i-1})u_i^2 - 2\sqrt{\beta\beta'}\sum_{i=1}^{L-1}\sqrt{q_i}u_i u_{i+1} \tag{3.51}$$

where the last line follows from the definition of $\tilde{J}$ and the smooth behaviour of q_i. One can show that the sequence s converges in a fast way, hence we can assume that in this interval of convergence the values assumed by q_i are around $q_0 = 1$. This permits us to substitute (3.49) into (3.51) obtaining

$$(u, M_{\text{sym}}u) \simeq \sum_{i=1}^{L} q_i u_i^2 - \sum_{i=1}^{L}(s_{i+1} - s_{i-1})u_i^2 - 2\sqrt{\beta\beta'}\sum_{i=1}^{L-1}\sqrt{q_i}u_i u_{i+1} = \tag{3.52a}$$

$$= \sum_{i=1}^{L} q_i u_i^2 - \frac{x_*}{x_0} + \frac{1}{x_0}\sum_{i=1}^{L-1} u_{i+1}u_i - \underbrace{2\sqrt{\beta\beta'}}_{\frac{1}{x_0}}\sum_{i=1}^{L-1}\sqrt{q_i}u_i u_{i+1} = \tag{3.52b}$$

$$= \sum_{i=1}^{L} q_i u_i^2 - \frac{x_*}{x_0} + \frac{1}{x_0}\sum_{i=1}^{L-1}(1 - \sqrt{q_i})u_{i+1}u_i \tag{3.52c}$$

Finally, in the infinite size limit $L \to +\infty$ the hopping rate function can be approximated to be the sum of the unity and a function that goes to zero as L^{-2} leading to

$$(u, M_{\text{sym}} u) = 1 - \frac{x_*}{x_0} \tag{3.53}$$

which represents the second upper bound

$$\lambda_{\min}^{(\infty)} \leq 1 - \frac{x_*}{x_0} \tag{3.54}$$

So far we have focused on two different upper bounds, therefore the minimum eigenvalue (slowest relaxation rate) in the infinite size limit needs to satisfy the tighter between the two, namely

$$\lambda_{\min}^{(\infty)} \leq \min \left\{ 1 - \frac{x_*}{x_0}, q_{\min} - 2\sqrt{q_{\min}\beta\beta'} \right\} \tag{3.55}$$

In particular, the numerical analysis reported in Figure 3.3 shows that the relation (3.55) is valid also as an equality; moreover, the absolute difference with the numerical computation is decreasing by increasing the size of the system as expected since approaching the thermodynamic limit. This implies that also a lower bound coincident to (3.55) exists.

3.1.3 Dynamical transition

In addition to the transitions in the stationary state between one phase to another of the homogeneous TASEP, there exists the so called dynamical transition as explained in Pelizzola and Pretti (2017). The latter does not correspond to any steady state transition and it is observed in the LD and HD phases. Considering the HD one, the transition can be characterized as follows: for any $\beta < \beta_{\text{HD/MC}}$, the slowest relaxation rate of the system is independent of α for any $\alpha \geq \alpha_c(\beta)$ where in the homogeneous case

$$\alpha_c(\beta) = \left[1 + \left(\frac{\beta}{1-\beta} \right)^{\frac{1}{3}} \right]^{-1} \tag{3.56}$$

while for $\alpha < \alpha_c(\beta)$ the relaxation rate depends on both α and β. This implies that the HD phase is divided in a so called slow region for $\alpha < \alpha_c(\beta)$ and a fast one for $\alpha \geq \alpha_c(\beta)$ at a given $\beta < \beta_{\text{HD/MC}}$. Due to the particle - hole symmetry of the system, the dynamical transition is also present in the LD phase with a symmetry with respect to the bisector $\alpha = \beta$ in the phase diagram. For this reason, it is

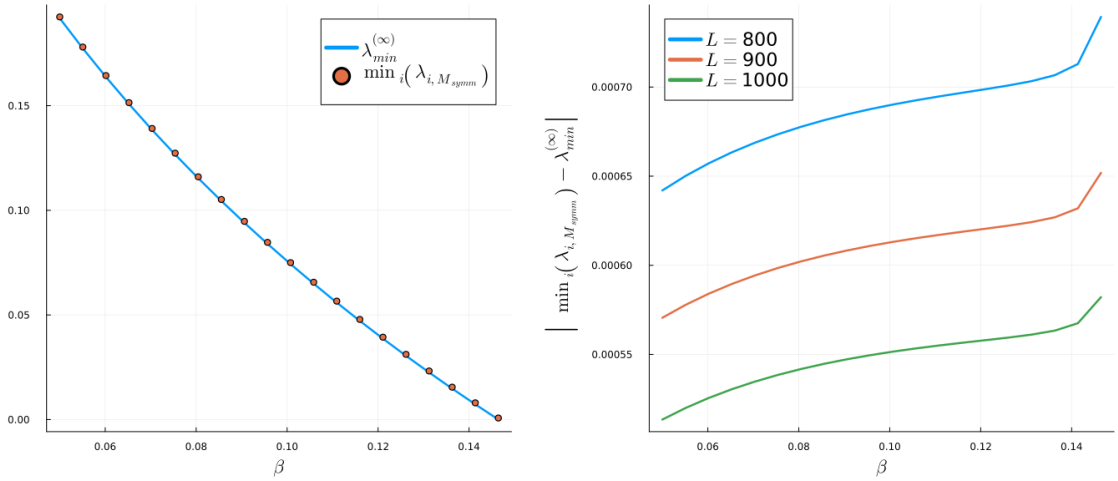

Figure 3.3: *Validity of the upper bound and in particular of equation* (3.55). *On the left there is the behaviour of the slowest relaxation rate (both with numerical analysis and analytical derivation) as a function of* β *till* $\beta_{HD/MC}$ *in order to investigate the HD phase with* $\alpha = 1, L = 800$ *and* $A = 1$. *On the right there is the absolute difference between the analytical and numerical version with increasing size of the system at* $\alpha = 1$ *and* $A = 1$.

convenient to focus our attention only in one phase, the HD one, for which we will characterize the dynamical transition.

We will see that the dynamical transition exists also in the inhomogeneous TASEP. An example, at finite size, of the behaviour of the slowest relaxation rate as a function of α is reported in Figure 3.4 where we can notice that from a certain α_c on the behaviour is independent on α, whereas below α_c we have to take into account the dependence on the entry rate. In particular, the curve for $A = 0$ shows a continuity in the first derivative at the critical point α_c; instead for the inhomogeneous case a discontinuity in the first derivative (corner point) at the critical entry rate is observed. The relaxation rate curves in the slow phase for the different values of A seem to collapse on a unique curve independently on A. Our objective is now to determine numerically the curve $\alpha_c(\beta)$ which characterizes the dynamical transition for the inhomogeneous model in order to generalize (3.56).

The determination of the critical value of the entry rate, that separates the slow and the fast region, is done in two different numerical ways. The first is based on an argument which involves the relation between the slowest relaxation rate at two different finite sizes with the one at infinite size; while the second involves the function $f(x)$ defined in (3.38).

- **First method**

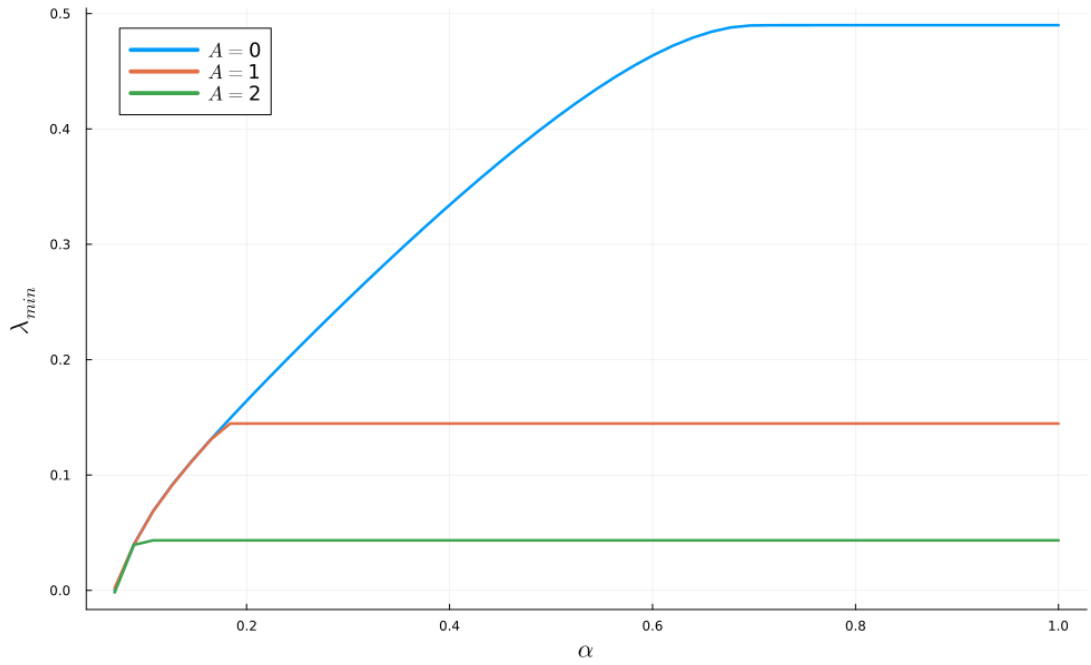

Figure 3.4: *Slowest relaxation rate in the HD phase at size* $L = 100$ *as a function of the entry rate* α *with* $\beta = 0.07$ *at different values of* A.

In the case of homogeneous TASEP and at a mean field level in the TASEP - LK, we know that the difference between the slowest relaxation rate at finite size $\lambda_{\min}^{(L)}$ and that at infinite size $\lambda_{\min}^{(\infty)}$ is asymptotically a power law in L. Assuming this behaviour also for the inhomogeneous TASEP,

$$\lambda_{\min}^{(L)} = \lambda_{\min}^{(\infty)} + kL^{-\gamma} \tag{3.57}$$

where k is a constant and $\gamma > 0$ is a suitable exponent. Taking two different sizes of the system L_1 and L_2 it is possible to solve the system

$$\begin{cases} \lambda_{\min}^{(L_1)} = \lambda_{\min}^{(\infty)} + kL_1^{-\gamma} \\ \lambda_{\min}^{(L_2)} = \lambda_{\min}^{(\infty)} + kL_2^{-\gamma} \end{cases} \tag{3.58}$$

with respect to $\lambda_{\min}^{(\infty)}$ which gives

$$\lambda_{\min}^{(\infty)} = \frac{\lambda_{\min}^{(L_2)} L_1^{-\gamma} - \lambda_{\min}^{(L_1)} L_2^{-\gamma}}{L_1^{-\gamma} - L_2^{-\gamma}} \tag{3.59}$$

The determination of γ is crucial because it enters in the $\lambda_{\min}^{(\infty)}$ expression and it is retrieved by fitting the difference between the relaxation rate at finite

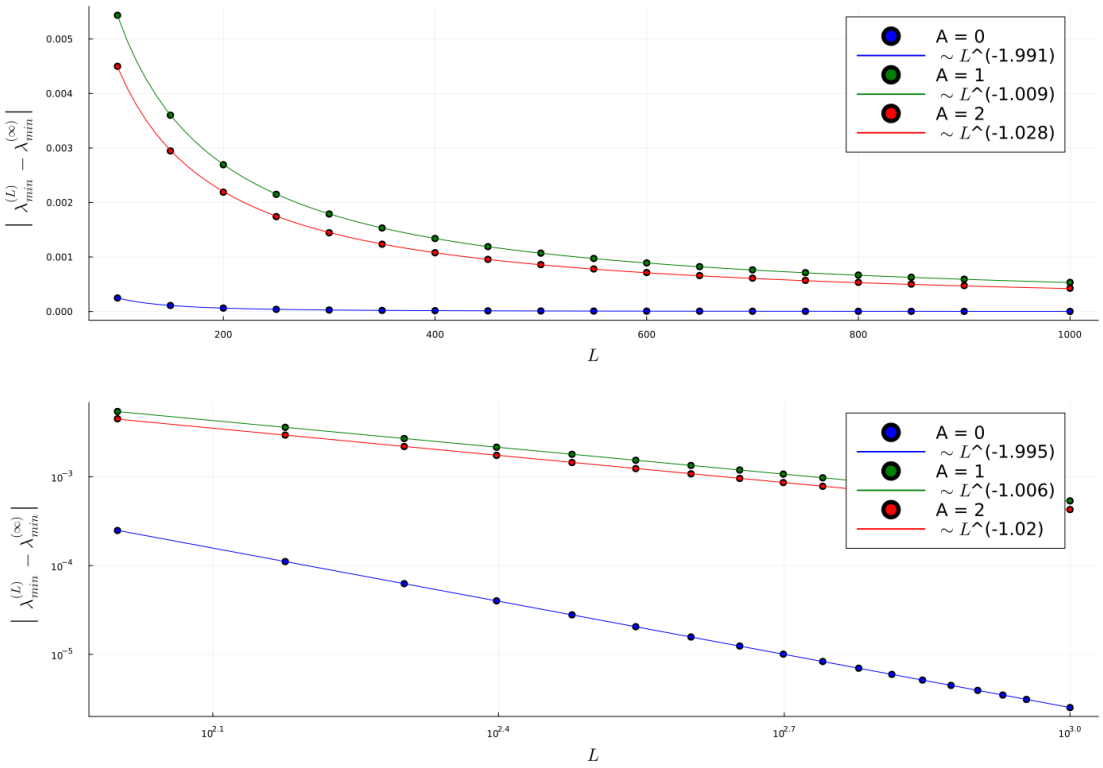

Figure 3.5: *Power law fitting with L of the difference between slowest relaxation rates at finite and infinite size for different values of A in the HD phase with $\alpha = 1$ and $\beta = 0.07$. On the top there is a lin - lin plot, instead at the bottom a log - log plot is shown.*

size and that at infinite size according to (3.55). The fitting is done in the HD phase for $A = 0, 1, 2$ as shown in Figure 3.5 where in the legend we can read the exponents γ.

In order to give an estimate of α_c it is sufficient to intersect the line $y = \lambda_{\min}^{(\infty)}$ with the profile of $\lambda_{\min}^{(L)}$ at the largest possible value of L. In this way we have a value of α_c for each value of $\beta < \beta_{\text{HD/MC}}$ and a related curve $\alpha_c(\beta)$. We will denote the critical value determined with this method with $\alpha_c^{(I)}$.

- **Second method**

It is possible to prove that the expression (3.55) acquires different behaviours

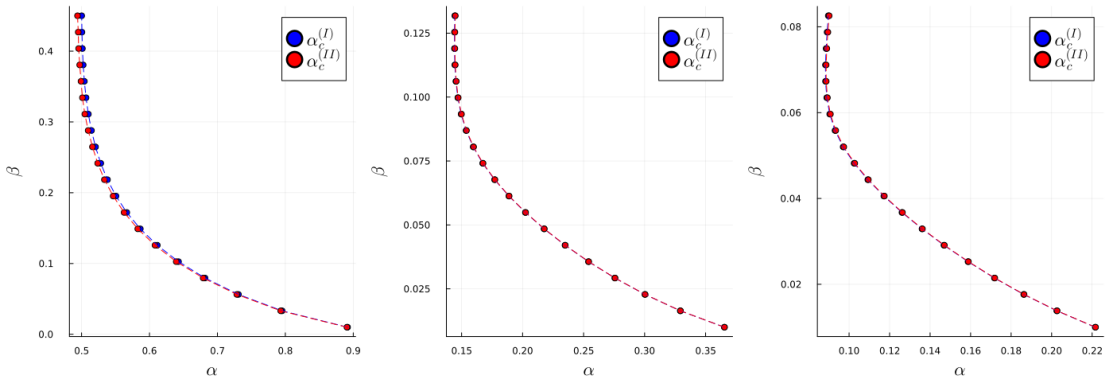

Figure 3.6: *Behaviour of α_c in the HD phase which characterizes the dynamical transition. From left to right, the curve refers to $A = 0, 1, 2$ with both methods described before.*

in the slow and fast regions. In particular

$$\lambda_{\min}^{(\infty)} = \begin{cases} 1 - \frac{x_*}{x_0}, & \alpha < \alpha_c \\ q_{\min} - 2\sqrt{q_{\min}\beta\beta'}, & \alpha > \alpha_c \end{cases} \tag{3.60}$$

The critical value of the entry rate α_c is retrieved when the two behaviours meet at

$$x_* = x_0(1 - q_{\min}) + 2x_0\sqrt{q_{\min}\beta\beta'} \tag{3.61}$$

and making use of (3.43), α_c is retrieved by imposing

$$f(x_*; \alpha_c, \beta) = 1 \tag{3.62}$$

which is solved numerically. We will denote the critical value determined with this method with $\alpha_c^{(II)}$.

The results from both methods for different values of A are reported in Figure 3.6 in which we can observe that for $A \neq 0$ the two methods coincide, whereas for the homogeneous case a little difference emerges. This happens because in the case of the smooth transition for $A = 0$, where the corner point is not present, the intersection between an horizontal line and an oblique one with small slope is more affected by numerical errors. It is interesting to observe that the curve of the critical entry rate, in the neighbourhood of $\beta_{\text{HD/MC}}$ becomes steeper and steeper with a recess.

3.2 Domain wall theory

The DWT describes the long term dynamics of driven systems in terms of two characteristic velocities, the domain wall or shock velocity v_s and the collective or group velocity v_g. In the case of the homogeneous TASEP model, DWT predicts the exact result in the slow phase. Following Dudzinski and Schütz (2000), we will generalize the domain wall description to the inhomogeneous TASEP. A domain wall, or shock, is a sharp interface connecting two phases at the stationary state. A shock separating two stationary phases of densities $\rho_i^{(-)}$ (on the left) and $\rho_{i+1}^{(+)}$ (on the right) moves with velocity

$$v_{i,i+1} = \frac{J_{i+1}^{(+)} - J_i^{(-)}}{\rho_{i+1}^{(+)} - \rho_i^{(-)}} \tag{3.63}$$

where the profiles $\rho^{(\pm)}$ are the discretization of bulk profiles (2.20b) and (2.22b)

$$\rho_i^{(-)} = \frac{1}{2}\left[1 - \sqrt{1 - \frac{4\alpha(1-\alpha)}{q_i}}\right], \qquad i = 1, \dots, L \tag{3.64a}$$

$$\rho_i^{(+)} = \frac{1}{2}\left[1 + \sqrt{1 - \frac{4\beta(1-\beta)}{q_i}}\right], \qquad i = 1, \dots, L \tag{3.64b}$$

and the current $J_i^{(\pm)}$ is instead the discretization of (2.16)

$$J_i^{(\pm)} = q_i \rho_i^{(\pm)} \left(1 - \rho_i^{(\pm)}\right), \qquad i = 1, \dots, L \tag{3.65}$$

The DWT can also provide a quantitative description of the relaxation toward the stationary state with the main assumption that the relaxation dynamics is determined by the shock diffusion, a random walk with (rightward, leftward) hopping rates given by

$$\begin{cases} D_i^{(+)} = \frac{J_i^{(+)}}{\rho_i^{(+)} - \rho_{i-1}^{(-)}}, & i = 1, \dots, L-1 \\ D_i^{(-)} = \frac{J_i^{(-)}}{\rho_{i+1}^{(+)} - \rho_i^{(-)}}, & i = 2, \dots, L \end{cases} \tag{3.66}$$

such that $v_{i,i+1} = D_{i+1}^{(+)} - D_i^{(-)}$ where

$$\rho_0^{(-)} = \alpha, \qquad \rho_{L+1}^{(+)} = 1 - \beta \tag{3.67}$$

The behaviour of random walk hopping rates for different values of A is reported in Figure 3.7 where we can notice that, as expected, in the homogeneous case the

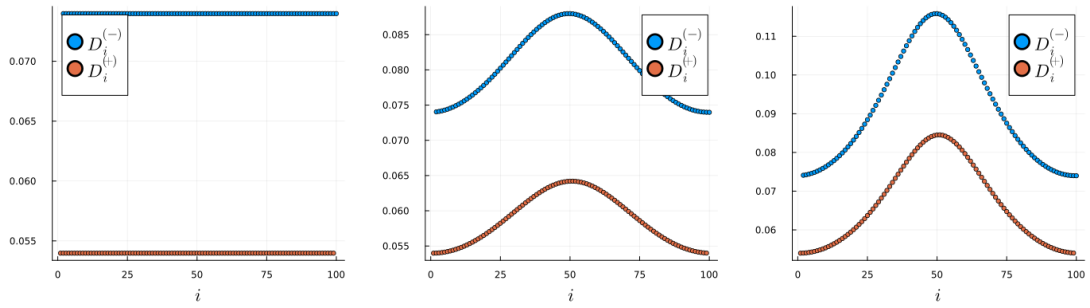

Figure 3.7: *Random walk (rightward and leftward) hopping rates in the HD phase with* $\alpha = 0.07, \beta = 0.05$ *and* $L = 100$ *for different values of* $A = 0, 1, 2$ *from left to right.*

random walk hopping rates are constant; whereas for $A \neq 0$ they depend on the lattice site with a maximum achieved in $i = \frac{L}{2}$.

Denoting by $\mathcal{P}_i(t)$ the probability that the shock is located at lattice site i at time t, the corresponding master equation for the shock position will be

$$\begin{cases} \dot{\mathcal{P}}_1(t) = D_2^{(-)}\mathcal{P}_2(t) - D_1^{(+)}\mathcal{P}_1(t) \\ \dot{\mathcal{P}}_i(t) = D_{i-1}^{(+)}\mathcal{P}_{i-1}(t) + D_{i+1}^{(-)}\mathcal{P}_{i+1}(t) - \left(D_i^{(-)} + D_i^{(+)}\right)\mathcal{P}_i(t), \qquad i = 2, 3, \dots, L-1 \\ \dot{\mathcal{P}}_L(t) = D_{L-1}^{(+)}\mathcal{P}_{L-1}(t) - D_L^{(-)}\mathcal{P}_L(t) \end{cases} \tag{3.68}$$

or more compactly in matrix form

$$\dot{\mathcal{P}}(t) = -\mathcal{M}\mathcal{P}(t), \qquad \mathcal{P}(t) = \begin{pmatrix} \mathcal{P}_1(t) \\ \vdots \\ \mathcal{P}_i(t) \\ \vdots \\ \mathcal{P}_L(t) \end{pmatrix} \tag{3.69}$$

where $\mathcal{M} \in \mathbb{R}^{L\times L}$ is tridiagonal with elements

$$\begin{cases} \mathcal{M}_{i,i} = \begin{cases} D_1^{(+)}, & i = 1 \\ D_i^{(-)} + D_i^{(+)}, & i = 2,3,\dots,L-1 \\ D_L^{(-)}, & i = L \end{cases} \\ \mathcal{M}_{i,i+1} = -D_{i+1}^{(-)}, \qquad i = 1,\dots,L-1 \\ \mathcal{M}_{i,i-1} = -D_{i-1}^{(+)}, \qquad i = 2,\dots,L \end{cases} \tag{3.70}$$

The latter is a quasi - Toeplitz matrix[5] in the case of homogeneous TASEP.

We are interested in the minimum (non vanishing) eigenvalue of $\mathcal{M}$ in the limit $L \to +\infty$ for the inhomogeneous TASEP where $\mathcal{M}$ in general is not a quasi - Toeplitz matrix, therefore we have to proceed numerically. Following an approach similar to section 3.1, we will use the QR decomposition (see Appendix A) of $\mathcal{M}$ in order to compute its spectrum and since the matrix is not symmetric, we will symmetrize it. The spectrum of $\mathcal{M}$ in the HD phase for $A = 1$ is shown in

[5] A matrix $\Xi \in \mathbb{R}^{L\times L}$ where each diagonal has a constant value except for the first and the last element of the main diagonal is said to be a quasi - Toeplitz matrix

$$\begin{cases} \Xi_{11} \equiv b \\ \Xi_{i+k,i} \equiv a_k, \qquad k = 0,1,2,\dots,L-1, \qquad i = 1,\dots,L-k \quad \wedge \quad (k,i) \neq (0,1),(0,L) \\ \Xi_{i,i+\kappa} \equiv a_{-\kappa}, \qquad \kappa = 1,2,\dots,L-1, \qquad i = 1,\dots,L-\kappa \\ \Xi_{LL} \equiv c \end{cases} \tag{3.71}$$

where $\{a_{\pm j}\}_{j=0}^{L-1} \in \mathbb{R}$ and $b \neq a_0, c \neq a_0$. Indeed, in the case of uniform hopping rates ($A = 0$), the random walk hopping rates are constant (see Figure 3.7) $D_i^{(+)} \equiv D_R$ and $D_i^{(-)} \equiv D_L$. The matrix $\mathcal{M}$ is quasi - Toeplitz with

$$\begin{cases} b = D_R, \quad a_0 = D_L + D_R, \quad c = D_L, \quad a_{-1} = -D_R, \quad a_1 = -D_L \\ a_j = 0, \quad \forall j = \pm 2, \pm 3, \dots, \pm(L-1) \end{cases} \tag{3.72}$$

and its minimum eigenvalue is given by

$$\lambda_1 = D_L + D_R - 2\sqrt{D_R D_L}\cos\frac{\pi}{L} \overset{L\to+\infty}{\longrightarrow} D_L + D_R - 2\sqrt{D_R D_L} \tag{3.73}$$

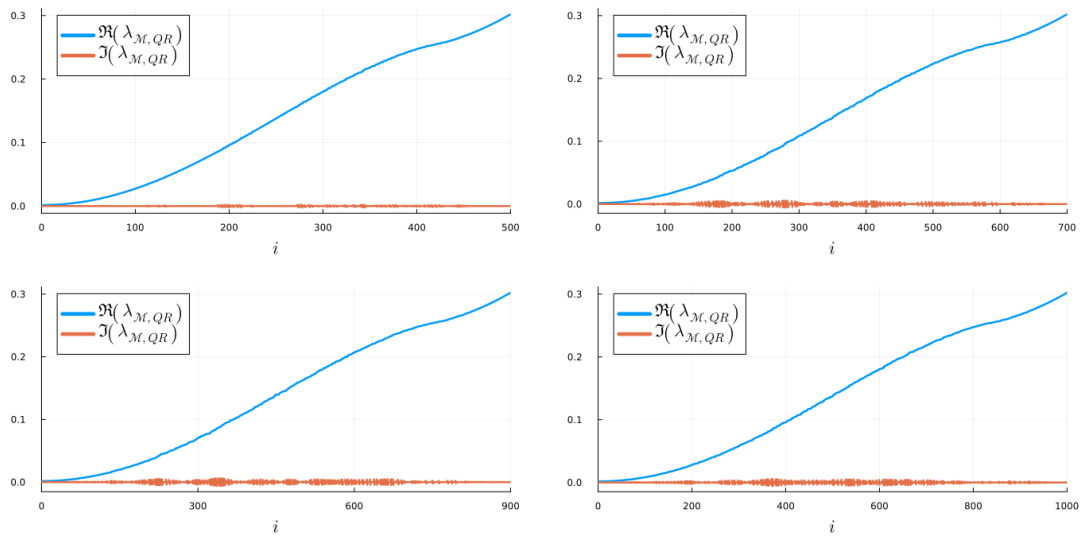

Figure 3.8: *Real and imaginary parts of the eigenvalues of $\mathcal{M}$ in HD phase computed with QR algorithm. The entry and exit rates are $\alpha = 0.07, \beta = 0.05$ and increasing size of the system $L = 500, 700, 900, 1000$.*

Figure 3.8 in which the real part of the eigenvalues is dominant with respect to the imaginary part. The latter is indeed a consequence of a numeric effect during the determination of the eigenvalues. We can symmetrize $\mathcal{M}$ in order to get rid of the numeric effect of the imaginary parts of the eigenvalues by following the same procedure as in the mean field case. In particular, we will obtain that the symmetrized matrix $\mathcal{M}_{\text{sym}}$ is tridiagonal with lower and upper diagonal

$$\begin{cases} (\mathcal{M}_{\text{sym}})_{i,i-1} = -\sqrt{D_{i-1}^{(+)} D_i^{(-)}}, & i = 2, \dots, L \\ (\mathcal{M}_{\text{sym}})_{i,i+1} = -\sqrt{D_i^{(+)} D_{i+1}^{(-)}}, & i = 1, \dots, L-1 \end{cases} \tag{3.74}$$

The spectrum of $\mathcal{M}_{\text{sym}}$ is completely real and it is in good agreement with the real part of the spectrum of $\mathcal{M}$ as Figure 3.9 shows.

The minimum (non vanishing) eigenvalue of $\mathcal{M}$ represents the slowest relaxation rate towards the stationary state in the DWT. We expect that its behaviour at a fixed β as function of α is qualitatively the one retrieved in the mean field case characterizing the dynamical transition. The numerical results for different values of A are illustrated in Figure 3.10 where the curve for $A = 0$ satisfies (3.73) and for the inhomogeneous case we notice an interval of α which is not accessible. This is due to the fact that $\rho_i^{(-)}$ exists only if

$$4\alpha(1-\alpha) \leq q_i, \qquad i = 0, \dots, L \tag{3.75}$$

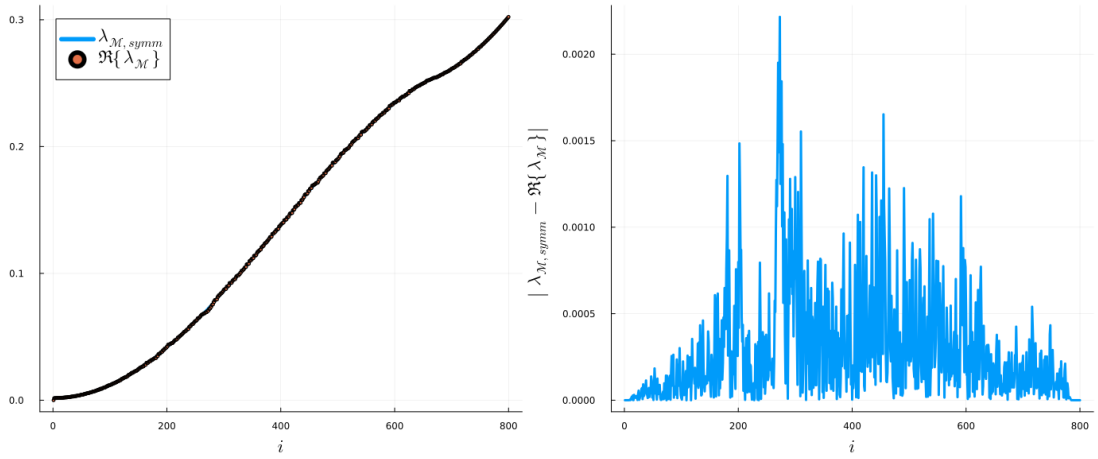

Figure 3.9: *Comparison between the spectrum of the symmetrized matrix* $\mathcal{M}_{sym}$ *with the real part of that of* $\mathcal{M}$ *in the HD phase with* $\alpha = 0.07, \beta = 0.05, A = 1, L = 800$. *On the left there is the entire spectrum, whereas on the right is shown the absolute difference between the two curves.*

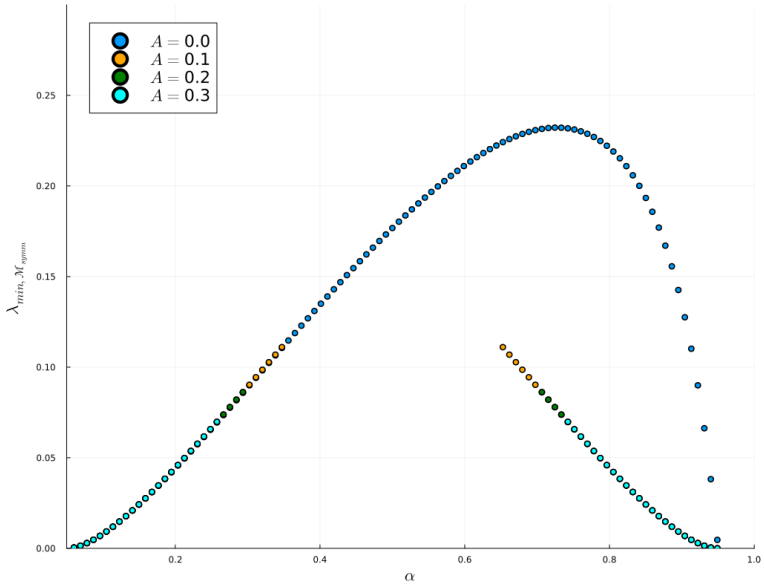

Figure 3.10: *Minimum (non vanishing) eigenvalue of* $\mathcal{M}_{sym}$ *with* $\beta = 0.05, L = 1000$ *for different values of* A.

as suggested by (3.64a). That condition is verified if the minimum of q_i is greater than $4\alpha(1-\alpha)$

$$\frac{1}{1+A} \geq 4\alpha(1-\alpha) \tag{3.76}$$

which implies that the intervals of α in the HD phase which are acceptable are the following

$$\beta \leq \alpha \leq \alpha_- \vee \alpha \geq \alpha_+, \qquad \alpha_\pm = \frac{1}{2}\left(1 \pm \sqrt{\frac{A}{1+A}}\right) \tag{3.77}$$

Clearly, for $A = 0$ we have $\alpha_\pm = \frac{1}{2}$ and therefore the whole range of α in the HD phase is covered. By increasing A we have that $\alpha_- \to 0$ and $\alpha_+ \to 1$ which implies that the forbidden range of α is wider and wider as shown in Figure 3.10.

We have tried to overcome this difficulty by replacing the profile $\rho_i^{(-)}$ with the non stationary profile for $\alpha \geq \alpha_-$. The non stationary mean field density profiles obey

$$\dot{\rho}_i(t) = q_{i-1}\rho_{i-1}(t)\Big(1-\rho_i(t)\Big) - q_i\rho_i(t)\Big(1-\rho_{i+1}(t)\Big), \qquad i = 1,\dots,L \tag{3.78}$$

with

$$\begin{cases} \rho_0(t) = \alpha \\ \rho_{L+1}(t) = 1-\beta \end{cases}, \quad \begin{cases} q_0 = 1 \\ q_L = 1 \end{cases} \tag{3.79}$$

The idea is now to use the non stationary density profiles in the DWT instead of the profile $\rho_i^{(-)}$ for $\alpha \geq \alpha_-$ maintaining β fixed. The numerical solution of (3.78) is reported in Figure 3.11 at different times for the same β and $\alpha = \alpha_- + 0.1$ in order to be sure that we are above α_-. We can observe that the stationary state is already reached at $t = 5200$ for $A = 0.1, 0.2, 0.3$ and at $t = 6000$ for $A = 0.4$, therefore we can choose any profile at $t \leq 5200$ to put in the DWT analysis. After some attempts, the best profile that gives the plateau like behaviour (as retrieved in the MFT) of $\lambda_{\min}$ (after a certain α_c) characterizing the dynamical transition is at $t = 2850$ from which the behaviour of the minimum eigenvalue is shown in Figure 3.12. The critical value α_c of the entry rate separating the slow from the fast region in the HD phase coincides with α_-. Unfortunately, the DWT approach does not provide any suggestion for the slowest relaxation rate of the inhomogeneous TASEP in infinite systems in terms of a closed form like the MFT prediction (3.55). However, this analysis has highlighted the fact that in the inhomogeneous TASEP there is a complex relaxation dynamics characterized by two different shocks (see Figure 3.11), qualitatively different from that of the homogeneous TASEP. Intuitively, this is explained by the fact that the dynamical transition in the inhomogeneous TASEP is of a different nature respect to that in the homogeneous model.

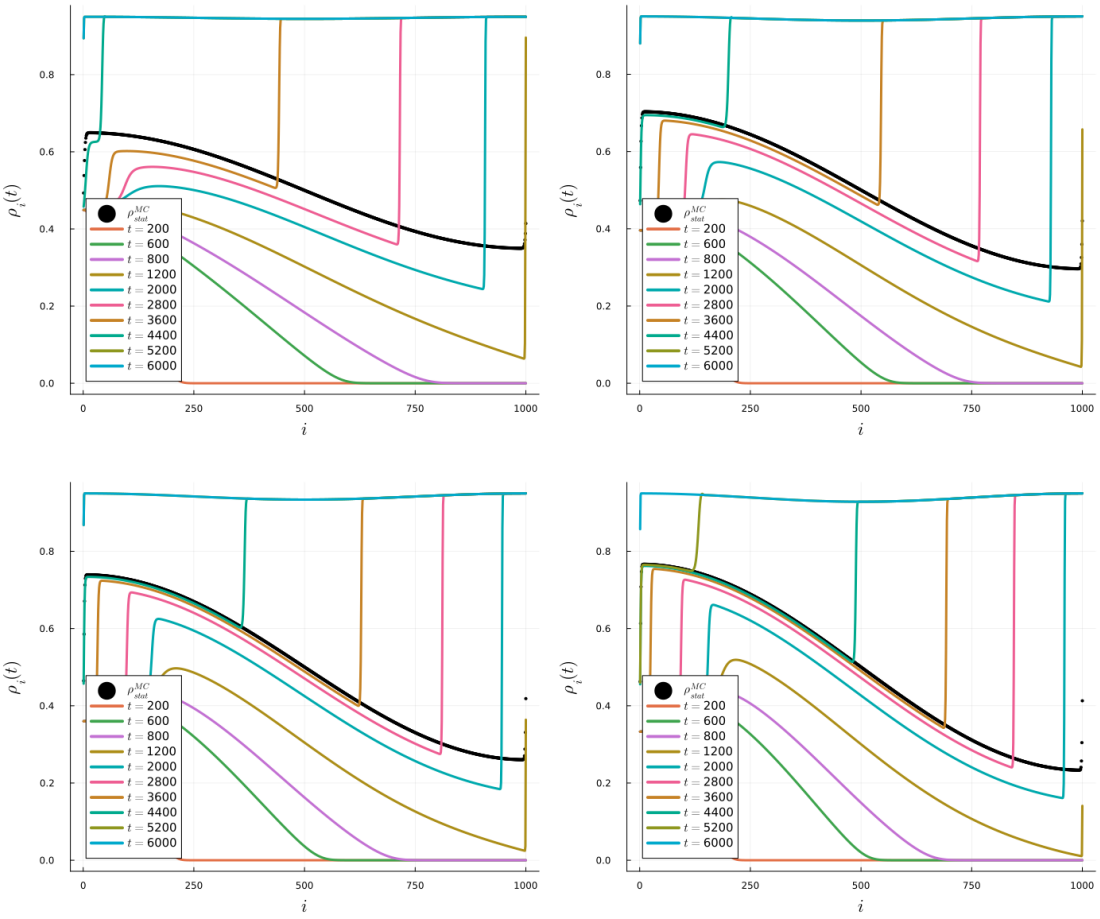

Figure 3.11: *Non stationary density profiles at different times with* $L = 1000, \beta = 0.05$ *and* $\alpha = \alpha_- + 0.1$ *for different values of* $A = 0.1, 0.2, 0.3, 0.4$ *from top left to bottom right. In each plot there is also shown the profile of the stationary MC state.*

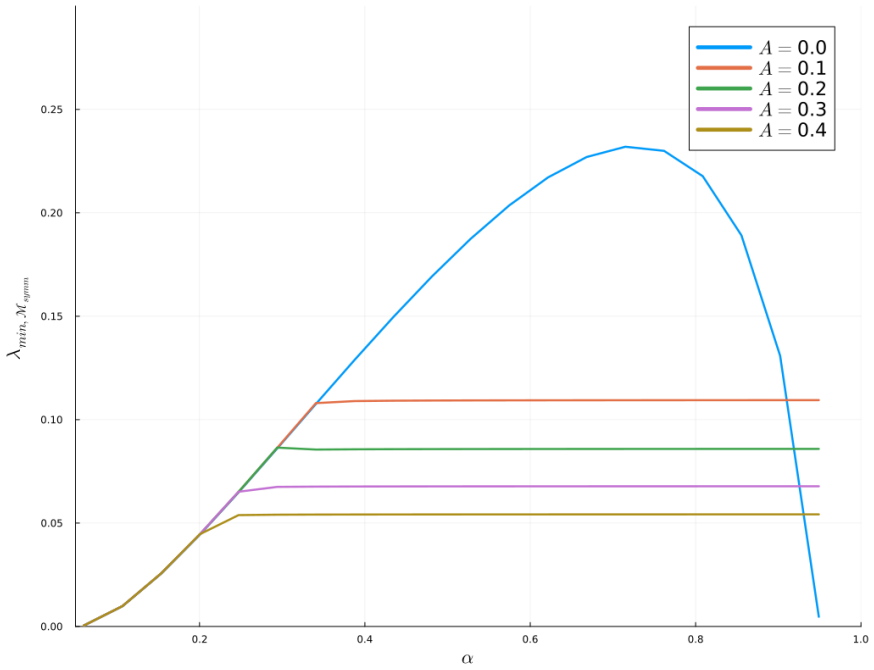

Figure 3.12: *Minimum (non vanishing) eigenvalue of* $\mathcal{M}_{sym}$ *with the non stationary density profile at* $t = 2850$ *instead of* $\rho_i^{(-)}$ *for* $\alpha \geq \alpha_-$ *with* $\beta = 0.05, L = 1000$ *and different values of* A.

3.3 A quantum approach

The relaxation times of the inhomogeneous TASEP can be calculated by diagonalizing the time evolution operator $\mathcal{H}$ of the process for finite systems as suggested in Dudzinski and Schütz (2000). We use the spin $\frac{1}{2}$ Pauli matrices $\sigma_k^{(x,y,z)}$ acting on site k of the chain

$$\sigma_k^{(x,y,z)} = \bigotimes_{i=1}^{k-1} \mathbb{I}_2 \otimes \sigma^{(x,y,z)} \otimes \bigotimes_{j=1}^{L-k} \mathbb{I}_2 = \tag{3.80a}$$

$$= \underbrace{\mathbb{I}_2 \otimes \ldots \otimes \mathbb{I}_2}_{k-1 \text{ times}} \otimes \sigma^{(x,y,z)} \otimes \underbrace{\mathbb{I}_2 \otimes \ldots \otimes \mathbb{I}_2}_{L-k \text{ times}} \tag{3.80b}$$

where $\otimes$ denotes the tensor product[6], $\mathbb{I}_2$ is the identity matrix 2×2 and $\sigma^{(x,y,z)}$ are the Pauli matrices

$$\sigma^{(x)} = \begin{pmatrix} 0 & 1 \\ 1 & 0 \end{pmatrix}, \qquad \sigma^{(y)} = \begin{pmatrix} 0 & -i \\ i & 0 \end{pmatrix}, \qquad \sigma^{(z)} = \begin{pmatrix} 1 & 0 \\ 0 & -1 \end{pmatrix} \tag{3.83}$$

with dimension $2^L \times 2^L$. Let us define the particle annihilation/creation operators

$$s_k^{(\pm)} = \frac{\sigma_k^{(x)} \pm i\sigma_k^{(y)}}{2} \tag{3.84}$$

and the projectors

$$n_k = \frac{1 - \sigma_k^{(z)}}{2} \tag{3.85}$$

on particles and

$$\nu_k = 1 - n_k \tag{3.86}$$

on vacancies. The generator $\mathcal{H}$ of the TASEP with non uniform hopping rates is closely related to a non Hermitian quantum Hamiltonian (whose dimension is $2^L \times 2^L$) of an anisotropic ferromagnetic spin $\frac{1}{2}$ Heisenberg chain

$$\mathcal{H} = \sum_{k=1}^{L-1} q_k \left(n_k \nu_{k+1} - s_k^{(+)} s_{k+1}^{(-)} \right) + \alpha \left(\nu_1 - s_1^{(-)} \right) + \beta \left(n_L - s_L^{(+)} \right) \tag{3.87}$$

[6]Given $A = \{a_{ij}\} \in \mathbb{R}^{m \times n}$ and $B = \{b_{kl}\} \in \mathbb{R}^{p \times q}$ the tensor product $\otimes$ between A and B is

$$A \otimes B \in \mathbb{R}^{mp \times nq} \tag{3.81}$$

with elements

$$(A \otimes B)_{(i,k),(j,l)} = a_{ij} b_{kl} \tag{3.82}$$

whose elements are the opposite with respect to the elements of the transition matrix. Indeed, all the contributions which appears in $\mathcal{H}$ with a minus in front correspond to the gain term in the master equation; whereas the contributions with a positive sign in $\mathcal{H}$ are the loss terms. In particular, for what it regards bulk process, the term $-q_k s_k^{(+)} s_{k+1}^{(-)}$ is a gain contribution, instead $q_k n_k \nu_{k+1}$ is a loss one (a similar argument can be applied for boundary terms too).

The goal is now determine the minimum (non vanishing) eigenvalue of the time evolution operator $\mathcal{H}$ at fixed β as a function of α in order to investigate the dynamical transition. The size of the matrix grows exponentially with L, hence the numerical eigenvalue evaluation is possible up to approximately 20 lattice sites which is too far from the condition $L \to +\infty$. For this reason, we will now describe a clever procedure to extract the minimum (non vanishing) eigenvalue of $\mathcal{H}$ for finite size and finally we will implement the FLE algorithm in order to access the thermodynamic limit.

Since the generator $\mathcal{H}$ is an asymmetric matrix, the numerical diagonalization is more difficult than in the standard case of symmetric or Hermitian matrices. Nevertheless there are methods which allow us to perform a numerically exact calculation of the eigenvalues. In particular, we will make use of the Arnoldi algorithm (see Appendix B) which is very efficient for large sparse matrices. Indeed, $\mathcal{H}$ has a lot of vanishing components with the advantage that the memory occupied is due only to the non zero entries. The peculiarity of the Arnoldi algorithm is that it does not determine the full spectrum, but only the minimum (non vanishing) eigenvalue.

The idea is to apply the Arnoldi algorithm to the evolution operator $\mathcal{H}$ for different sizes (we considered sizes from $L = 10$ to $L = 20$) and then extrapolate the smallest relaxation rate in the limit $L \to +\infty$. In Figure 3.13 we can see an example of the behaviour of $\lambda_{\min}$ at fixed β as a function of α where increasing the size the expected plateau decreases. In order to collect enough data, the smallest relaxation rate evaluation as function of α is done for $\beta = 0.1, 0.15$ and $\beta = 0.2$ for each value of $A = 0, 0.1, 0.2$ and $A = 0.3$. In some of these cases, we have noticed that, for specific sizes, the curve of the slowest relaxation rate shows spikes as reported inFigure 3.14. The spikes appearing in the curves are due to numerical effects and we will see how to treat them in the FLE algorithm.

3.3.1 Bulirsch and Stoer algorithm

Inspired by Henkel and Schutz (1988), we apply the Bulirsch and Stoer algorithm in order to investigate the slowest relaxation rate in the thermodynamic limit as function of α with the associated dynamical transition.

The Bulirsch and Stoer algorithm is a FLE algorithm useful to extrapolate finite size data towards the thermodynamic limit $L \to +\infty$. In order to describe

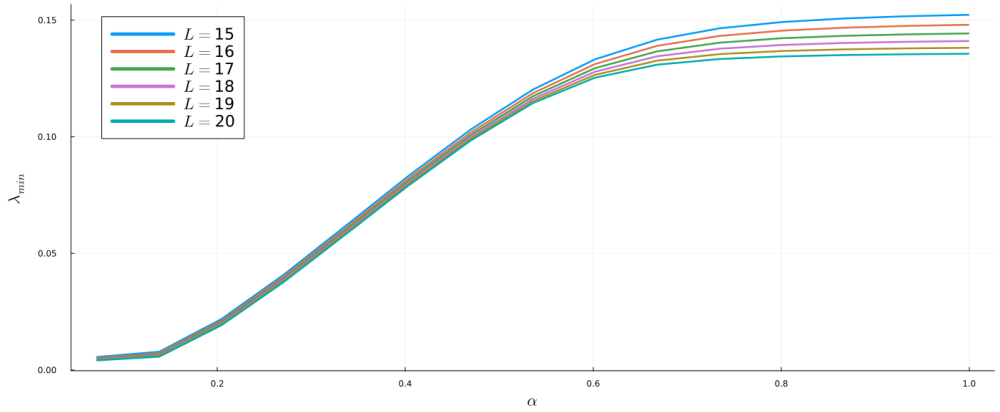

Figure 3.13: *Behaviour of the minimum (non vanishing) eigenvalue of the evolution operator $\mathcal{H}$ for different sizes as function of α for $\beta = 0.1$ and $A = 0.1$.*

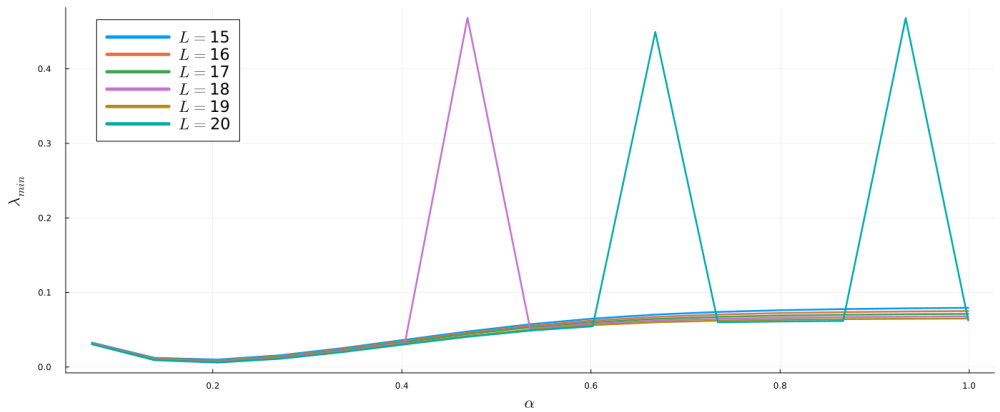

Figure 3.14: *Behaviour of the minimum (non vanishing) eigenvalue of the evolution operator $\mathcal{H}$ for different sizes as function of α for $\beta = 0.2$ and $A = 0.1$.*

it, let us define

- $\mathcal{L}$ as the set of all possible finite sizes considered for which we have determined the slowest relaxation rate with the Arnoldi algorithm. As explained before, we have computed data from $L = 10$ to $L = 20$

$$\mathcal{L} = \{10, 11, \ldots, 20\} \tag{3.88}$$

  whose cardinality is denoted by N and its elements by l_i in such a way that $\mathcal{L} = \{l_i\}_{i=1}^{N}$.

- ω as a free parameter whose choice is non trivial as we will see.

The desired thermodynamic limit $\lambda_{\min}^{(\infty)}$ is obtained from the following table of extrapolants

$$\begin{array}{ccccccc}
T_0^{(l_1)} & & & & & & \\
 & T_1^{(l_1)} & & & & & \\
T_0^{(l_2)} & & T_2^{(l_1)} & & & & \\
\vdots & T_1^{(l_2)} & \vdots & \ddots & & & \\
\vdots & \vdots & \vdots & & & & \\
T_0^{(l_j)} & T_1^{(l_k)} & T_2^{(l_h)} & \cdots & T_{N-1}^{(l_1)} & & \\
\vdots & \vdots & \vdots & & & & \\
\vdots & \vdots & T_2^{(l_{N-2})} & \iddots & & & \\
\vdots & T_1^{(l_{N-1})} & & & & & \\
\vdots & & & & & & \\
T_0^{(l_N)} & & & & & &
\end{array} \tag{3.89}$$

where $T_m^{(l_i)}$ are recursive quantities whose definition is

$$\begin{cases}
T_{-1}^{(l)} = 0, & l \in \mathcal{L} \\
T_0^{(l)} = \lambda_{\min}^{(l)}, & l \in \mathcal{L} \\
T_m^{(l_i)} = T_{m-1}^{(l_{i+1})} + \dfrac{T_{m-1}^{(l_{i+1})} - T_{m-1}^{(l_i)}}{\left(\frac{l_{i+m}}{l_i}\right)^{\omega} \cdot \left(1 - \frac{T_{m-1}^{(l_{i+1})} - T_{m-1}^{(l_i)}}{T_{m-1}^{(l_{i+1})} - T_{m-2}^{(l_{i+1})}}\right) - 1}, & m = 1, \ldots, N-1 \quad , \quad i = 1, \ldots, N-m
\end{cases} \tag{3.90}$$

with $\lambda_{\min}^{(L)}$ the slowest relaxation rate of the system with size L at a given α, β and A whose finite size behaviour is assumed to be

$$\lambda_{\min}^{(L)} = \lambda_{\min}^{(\infty)} + \frac{a_1}{L^{\omega}} + \frac{a_2}{L^{2\omega}} + \dots \tag{3.91}$$

The desired thermodynamic limit $\lambda_{\min}^{(\infty)}$ at the same parameters is then obtained by the rightmost cell of the table of extrapolants $T_{N-1}^{(l_1)}$. This happens because the entries in column i start to converge faster and faster, with respect to the entries in column $i-1$, to a unique value that is the extrapolated result $T_{N-1}^{(l_1)}$. The table of extrapolants needs to be constructed for each value of α (with β and A fixed) where the first column, as dictated by the recursion (3.90), contains the slowest relaxation rate at finite size for that particular α.

The extrapolated slowest relaxation rate in the thermodynamic limit $\lambda_{\min}^{(\infty)}$ is strongly dependent on the choice of the free parameter ω. An intrinsic criterion for choosing it is that of minimizing the difference between two consecutive elements of the column m in the table of extrapolants. In particular, we can define

$$\varepsilon_m^{(i)} = 2\left(T_m^{(i+1)} - T_m^{(i)}\right) \tag{3.92}$$

a quantity which needs to be minimized. It is quite intuitive that, if we want to ensure a good convergence of the algorithm, $\varepsilon_m^{(i)}$ needs to be ideally zero, meaning that two consecutive elements on the column m are exactly equal. However, this criterion for choosing ω is not so reliable because $\varepsilon_m^{(i)}$ is defined for all the N columns of the table of extrapolants and for each couple of adjacent elements (except for the last column where only the extrapolated value is present). The total number of possible values of $\varepsilon_m^{(i)}$ is

$$\sum_{j=1}^{N-1}(N-j) = \binom{N}{2} \tag{3.93}$$

for each table of extrapolants (hence, for each value of α). In our case where $N = 10$, we have 45 values of $\varepsilon_m^{(i)}$ that need to be minimized in order to choose the best ω. For this reason it is not a well defined problem to solve and in our analysis we have made only a minimization of $\varepsilon_{N-1}^{(i)}$ which is related to the second last column (that is the most important one since it is the column before the extrapolated value). In Figure 3.15 we show the behaviour of $\varepsilon_{N-1}^{(i)}$ as function of ω. We can notice that the minimization is not so accurate because there are other values of ω for which $\varepsilon_{N-1}^{(i)}$ is very close to the minimum found numerically. Doing the minimization of $\varepsilon_{N-1}^{(i)}$ for all values of α we obtain a distribution of the best ω reported in Figure 3.16. It is expected that the finite size scaling is characterized by an exponent ω which is independent on A, α and β, therefore this is clearly

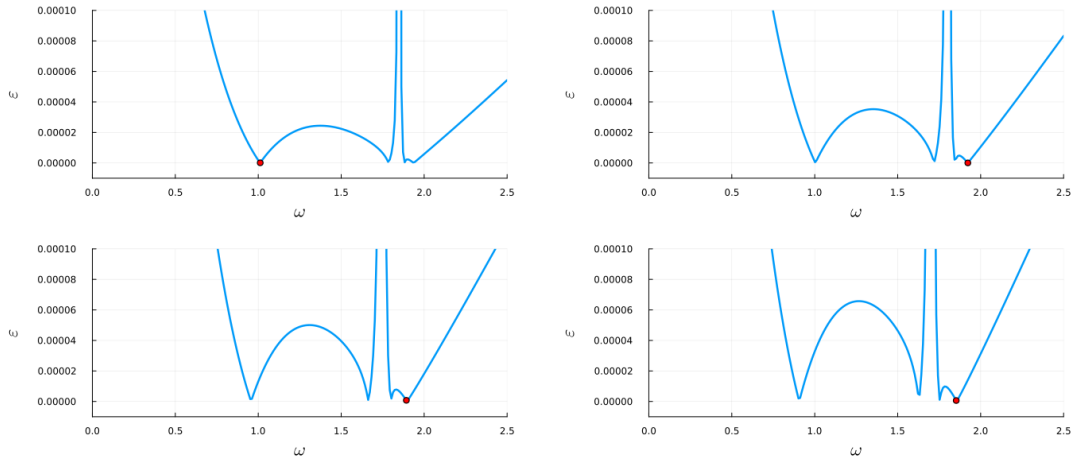

Figure 3.15: *Behaviour of* $\varepsilon_{N-1}^{(i)}$ *(solid line) as function of* ω *for* $\beta = 0.2, A = 0.1$ *and* $\alpha = 0.072, 0.138, 0.205, 0.271$ *from top left to bottom right. The marker shows the point for which* $\varepsilon_{N-1}^{(i)}$ *is minimum.*

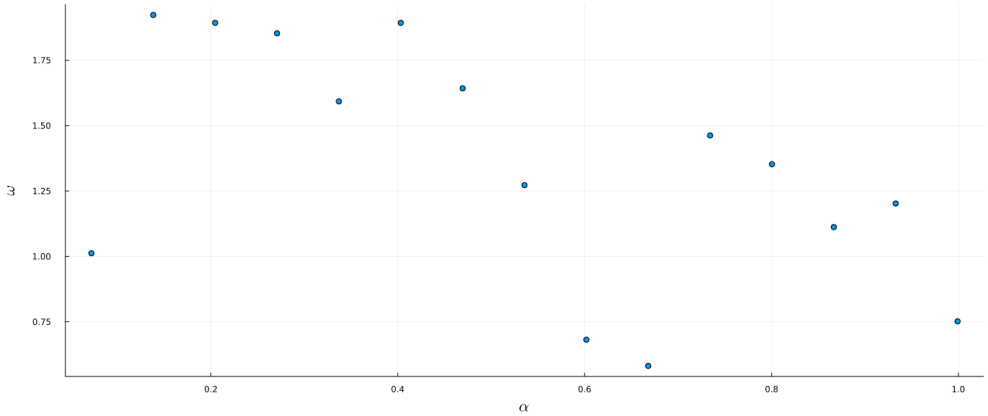

Figure 3.16: Distribution of the best ω minimizing $\varepsilon_{N-1}^{(i)}$ as function of α for $\beta = 0.2$ and $A = 0.1$.

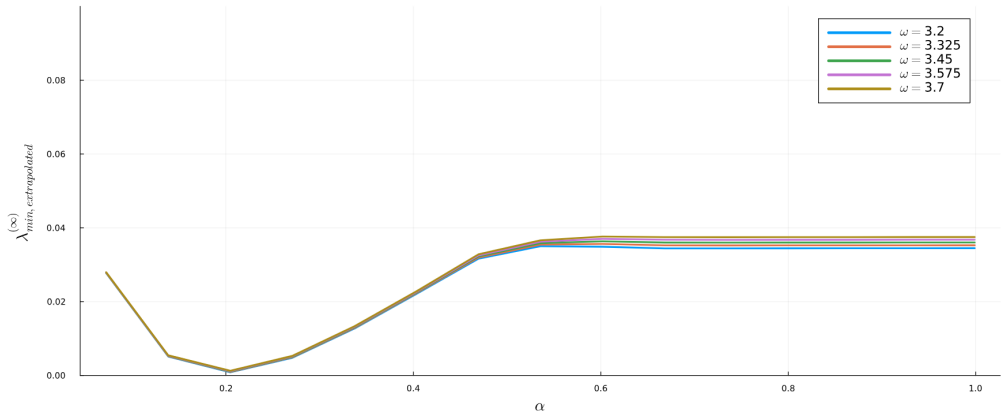

Figure 3.17: *Slowest extrapolated relaxation rate at infinite size as function of* α *for* $\beta = 0.2, A = 0.1$ *and different free parameters* ω*.*

β \ A	0	0.1	0.2	0.3
0.1	1.5	3.4	4.4	4.7
0.15	1.45	3.4	4.4	4.7
0.2	1.4	3.4	2.7	2.9

Table 3.1: ω *as a function of* β *and* A *in such a way to obtain the best plateau of* $\lambda_{min}^{(\infty)}$ *by visual inspection in the Bulirsch and Stoer algorithm.*

in contrast with our obtained result. This shows that the intrinsic criterion for choosing ω in such a way to minimize $\varepsilon_{N-1}^{(i)}$ is not so accurate. One could think that this happens because for $\beta = 0.2$ and $A = 0.1$ the finite size eigenvalue calculation (see Figure 3.14) shows some spikes; however a similar non constant behaviour of ω is obtained also for $\beta = 0.1$ and $A = 0.1$ where the eigenvalue behaviour at finite size does not present any spikes (see Figure 3.13). Moreover the present behaviour of ω with this intrinsic criterion is in common in all the analysed cases for $\beta = 0.1, 0.15, 0.2$ and $A = 0, 0.1, 0.2, 0.3$.

In order to overcome this problem, we have tried to set a unique value of ω in such a way to obtain the plateau like behaviour of $\lambda_{\text{min}}^{(\infty)}$ as in MFT and DWT. In Figure 3.17 the profile of $\lambda_{\text{min}}^{(\infty)}$ is shown as a function of the entry rate α with different values of ω. It can be noticed that varying ω changes slightly the plateau level of the slowest relaxation rate at infinite size. In particular, the specific ω is chosen to be the one that gives the best plateau by simple visual inspection: all the retrieved values are reported in Table 3.1 depending on the choice of β and A. We can observe that at fixed A, ω is almost constant with β except for $A = 0.2$

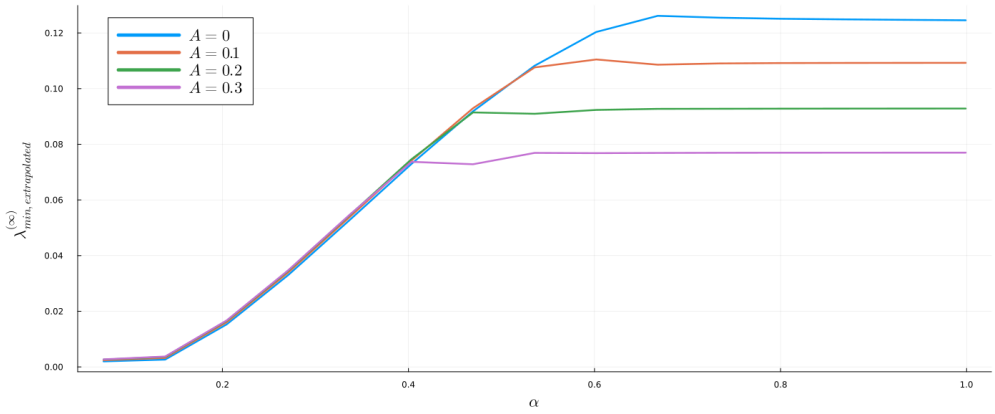

Figure 3.18: *Slowest extrapolated relaxation rate at infinite size as function of* α *for* $\beta = 0.1$ *and different values of* A.

and $A = 0.3$ where the values related to $\beta = 0.2$ are considerably different from those at $\beta = 0.1$ and $\beta = 0.15$. The profile of the extrapolated slowest relaxation rate at $\beta = 0.1$ as function of α with the related ω free parameter in Table 3.1 is reported in Figure 3.18. This result (a very similar behaviour is observed also for $\beta = 0.15$ and $\beta = 0.2$) is in agreement with the profiles obtained in MFT and DWT where for $A \neq 0$ the $\lambda_{\min}^{(\infty)}$ profile coincides with that of the homogeneous case up to the critical value α_c separating the slow from the fast region. Note that in the homogeneous TASEP case the extrapolate slowest relaxation rate is very close to the one predicted in the DWT by (3.73) as a confirmation of the Bulirsch and Stoer algorithm (at least in the $A = 0$ case). The latter observation permits us to determine the critical value α_c by intersecting the plateau level λ_{plateau} (actually we have taken a mean since there is still some variation as reported in Figure 3.18) with the exact result (3.73) which, as a function of α (at fixed β), reads

$$\lambda_1(\alpha;\beta) = \frac{\alpha(1-\alpha)+\beta(1-\beta)}{1-\beta-\alpha} - \frac{2}{1-\beta-\alpha}\sqrt{\alpha(1-\alpha)\beta(1-\beta)} \tag{3.94}$$

Solving numerically the equation

$$\lambda_1(\alpha_c;\beta) = \lambda_{\text{plateau}} \tag{3.95}$$

for all the values of β and A analysed leads us to Figure 3.19 where we report the curve separating the slow from the fast region in the α/β plane.

In order to have a confirmation of the Bulirsch and Stoer algorithm results, a last (very intuitive) method was implemented. It is know that the slowest relaxation rate of the homogeneous TASEP at finite size has an expansion in powers of

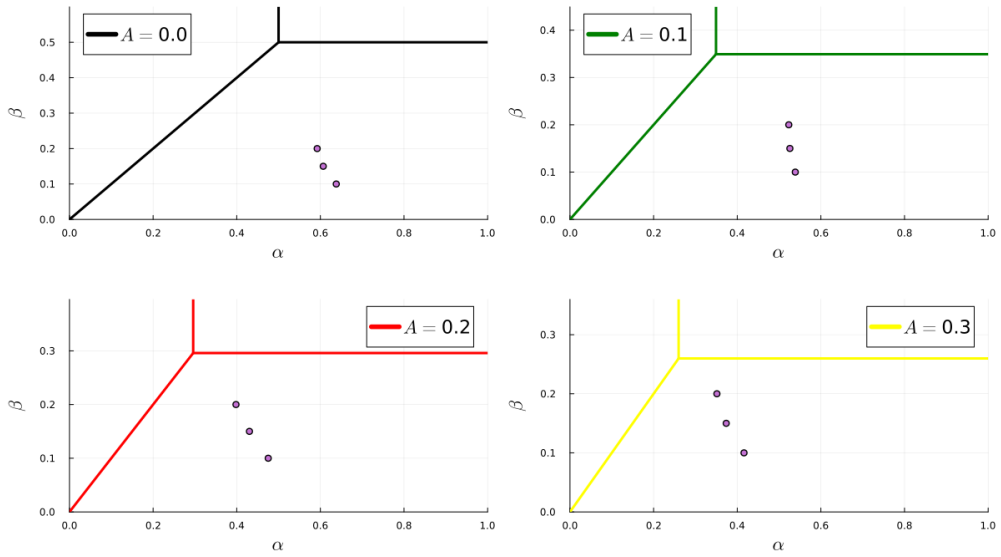

Figure 3.19: *Critical entry rates in the HD phase describing the dynamical transition with the FLE technique for* $A = 0, 0.1, 0.2$ *and* $A = 0.3$ *from top left to bottom right.*

$\frac{1}{L}$

$$\lambda_{\min}^{(L)} = \lambda_{\min}^{(\infty)} + \sum_{j=1}^{+\infty} \frac{\lambda_j}{L^j} \tag{3.96}$$

with $\lambda_1 = 0$ and $\{\lambda_j\}_{j=2}^{\infty}$ a sequence of real numbers. The idea is to assume the expansion to be valid also for the inhomogeneous model we are focused on and fit the data that we have retrieved at finite size to (3.96). The fit was done truncating (3.96) to fourth order ($j = 4$). In Figure 3.20 we show the results for $\beta = 0.1$. Comparing Figure 3.20 with Figure 3.18, the former shows a more regular plateau than the latter for different values of A. However, the obtained plateau level is qualitatively comparable in both cases as Table 3.2 shows.

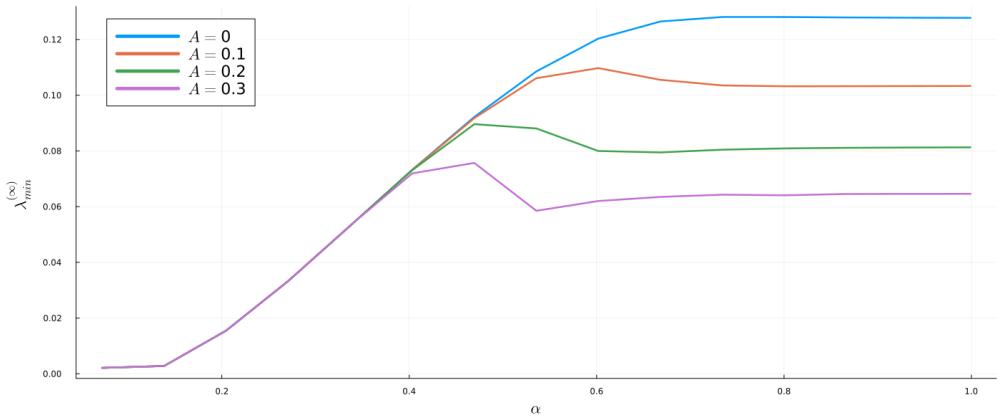

Figure 3.20: *Slowest relaxation rate at infinite size as function of α for $\beta = 0.1$ and different values of A retrieved by fitting the finite size data.*

$\boldsymbol{\beta}$ \ **A**	0	0.1	0.2	0.3
0.1	3.3×10^{-3}	5.7×10^{-3}	1.1×10^{-2}	1.2×10^{-2}
0.15	3.8×10^{-3}	5.6×10^{-3}	4.7×10^{-3}	5.4×10^{-3}
0.2	3.6×10^{-3}	5.3×10^{-3}	1.1×10^{-3}	2.6×10^{-3}

Table 3.2: *Difference, in absolute value, between the plateau level retrieved within the Bulirsch and Stoer algorithm and the one by fitting the finite size data.*

Chapter 4

Conclusions

In the present work we have described in detail the relaxation process of the inhomogeneous TASEP model towards the stationary state with the main interest in the dynamical transition in the thermodynamic limit. After an analysis of the stationary state itself, we have used three methods to obtain the behaviour of the slowest relaxation rate as a function of the entry rate α and to locate the dynamical transition, which separates the slow from the fast region in the HD phase

- MFT that leads us to obtain two analytical upper bounds of the slowest relaxation rate in infinite system size. The latter has to satisfy the tightest bound and moreover a numerical evaluation seems to indicate that the bound is satisfied as an equality. This suggests that a lower bound coincident with the upper bound exists as in the case of TASEP - LK with uniform hopping rates (see Botto et al. (2020)).

- DWT that does not provide any analytical results (excepts for the homogeneous TASEP model). Considering a standard domain wall between two different phases at stationarity, we observed that a region of α is inaccessible in the behaviour of the slowest relaxation rate in the thermodynamic limit. The latter issue was resolved by taking into account a domain wall description with a non stationary state for which the obtained result is qualitatively in agreement with the behaviour suggested by MFT.

- FLE algorithm (Bulirsch and Stoer) applied to the quantum approach description of the model. In particular, the slowest relaxation rate of the inhomogeneous TASEP model was calculated by diagonalizing a specific time evolution operator whose size is exponential in the size of the system. For this reason, in order to inspect the thermodynamic limit, we made use of the Bulirsch and Stoer algorithm which extrapolates the slowest relaxation rate at infinite size from finite size results computed with the help of the Arnoldi

algorithm. This approach is numerically consistent with the result obtained by fitting the finite size data as suggested by the homogeneous TASEP.

We can conclude that all the presented methods give the same qualitative description of the slowest relaxation rate of the system as function of the entry rate α in the thermodynamic limit. The dynamical transition in the HD phase is well described with the corresponding curve separating the slow from the fast region. Due to the particle - hole symmetry of the model, the transition is automatically described also in the LD phase of the system where the curve separating the slow from the fast region is symmetric with respect to the line $\alpha = \beta$ in the phase diagram.

Especially the diagonalization of the evolution operator using the Bulirsch and Stoer algorithm could be improved in future works in order to preserve the constant finite size scaling of the slowest relaxation rate through a clever criterion than the visual inspection used here. Actually, an intrinsic criterion was described, however it is not well defined and leads to a non constant behaviour of the finite size scaling as a function of α. In particular, since we expected it to be independent of α, we have tried a set of values up to obtain qualitatively the plateau after a certain α_c. Despite the fact that the latter was used, the FLE algorithm shows good results, which agree with those obtained by MFT and DWT.

Appendix A

QR algorithm

Any square matrix $A \in \mathbb{R}^{L\times L}$ may be decomposed as

$$A = QR \tag{A.1}$$

where Q is an orthogonal matrix[7] and R is an upper triangular matrix.

In particular this decomposition is useful to retrieve the eigenvalues of a generic matrix A. Let

$$A_0 = A \tag{A.2}$$

and at the k-th step (starting with $k = 0$) we compute the QR decomposition

$$A_k = Q_k R_k \tag{A.3}$$

We then form

$$A_{k+1} = R_k Q_k \tag{A.4}$$

which can be written, thanks to A.3

$$\begin{aligned} A_{k+1} &= R_k Q_k = && \text{(A.5a)}\\ &= Q_k^{-1} A_k Q_k = && \text{(A.5b)}\\ &= Q_k^T A_k Q_k && \text{(A.5c)} \end{aligned}$$

due to the orthogonality of Q.

This means that all the A_k are similar and hence have the same eigenvalues. Under certain conditions, the matrices A_k converge to a triangular matrix, the so

[7]There is also a generalization to a matrix $A \in \mathbb{C}^{L\times L}$ where Q is a unitary matrix satisfying $Q^\dagger = Q^{-1}$.

called Schur form of A, whose eigenvalues are listed over the diagonal. The eigenvalue problem is therefore solved since at a certain $k = \kappa$ we reach the Schur form and the spectrum of A_κ coincides with that of $A_0 = A$. Moreover, the algorithm is numerically stable because it proceeds by orthogonal similarity transformations.

The algorithm can be applied to the relaxation matrix $M \in \mathbb{R}^{L\times L}$ and one of the conditions that leads to a Schur form is the fact that M is tridiagonal with non zero off diagonal entries (indeed M is irreducible). Thanks to this, κ is reached in a finite time and the algorithm converges.

Appendix B

Arnoldi algorithm

The Arnoldi algorithm is an iterative algorithm for eigenvalues and eigenvectors of general (possibly non Hermitian) matrices consisting in Arnoldi iterations. It is based on the construction of an orthonormal basis of the Krylov subspace[8], which makes it particularly useful when dealing with large sparse matrices.

The Arnoldi iteration produces a sequence of orthonormal vectors (Arnoldi vectors) $q_1, q_2, \ldots, q_n$ such that for every i, the vectors $q_1, \ldots, q_i$ span the Krylov subspace $\mathcal{K}_i$. The algorithm stops when q_k is the zero vector as compactly described in 1

Algorithm 1 Arnoldi algorithm

Require: arbitrary vector q_1 with norm 1
  while $q_k \neq 0$ **do**
    $q_k \leftarrow A^{-1}q_{k-1}$
    for $j = 1 : k-1$ **do**
      $h_{j,k-1} \leftarrow q_j^* q_k$
      $q_k \leftarrow q_k - h_{j,k-1}q_j$
    end for
    $h_{k,k-1} \leftarrow \|q_k\|$
    $q_k \leftarrow \frac{q_k}{h_{k,k-1}}$
  end while

[8]The order r Krylov subspace generated by $A \in \mathbb{R}^{n\times n}$ and $b \in \mathbb{R}^{n\times 1}$ is the linear subspace spanned by the images of b under the first r powers of A

$$\mathcal{K}_r(A, b) = \mathbf{span}\left\{b, Ab, A^2b, \ldots, A^{r-1}b\right\} \tag{B.1}$$

The Arnoldi process needs b to get started which typically, for eigenvalue problems, it is assumed to be random.

In particular, let $A \in \mathbb{R}^{m\times m}$ be the large sparse matrix whose eigenvalues we want to determine and $Q_n \in \mathbb{R}^{m\times n}$ formed by the first n Arnoldi vectors $q_1, \dots, q_n$. Define

$$H_n = Q_n^* A^{-1} Q_n = \begin{pmatrix} h_{11} & h_{12} & h_{13} & \dots & h_{1n} \\ h_{21} & h_{22} & h_{23} & \dots & h_{2n} \\ 0 & h_{32} & h_{33} & \dots & h_{3n} \\ \vdots & \ddots & \ddots & \ddots & \vdots \\ 0 & \dots & 0 & h_{n,n-1} & h_{nn} \end{pmatrix} \tag{B.2}$$

the upper Hessenberg matrix with non vanishing elements h_{jl} computed in the algorithm. Since $H_n \in \mathbb{R}^{n\times n}$ has a modest size, its eigenvalues (called Ritz eigenvalues) can be computed efficiently using the QR algorithm (see Appendix A). It is observed that some of the eigenvalues of H_n (at most n in total) converge to the smallest eigenvalues of A (at most $m > n$ in total).

In our application, the algorithm is very useful since we have to compute the second smallest eigenvalue (because the smallest one is known to be zero) of the evolution operator $\mathcal{H}$.

List of Figures

Bibliography

Botto, D., Pelizzola, A., Pretti, M., and Zamparo, M. (2018). Dynamical transition in the tasep with langmuir kinetics: mean-field theory. *Journal of Physics A: Mathematical and Theoretical*, 52(4):045001.

Botto, D., Pelizzola, A., Pretti, M., and Zamparo, M. (2020). Unbalanced langmuir kinetics affects tasep dynamical transitions: mean-field theory. *Journal of Physics A: Mathematical and Theoretical*, 53(34):345001.

Dudzinski, M. and Schütz, G. (2000). Relaxation spectrum of the asymmetric exclusion process with open boundaries. *Journal of Physics A: Mathematical and General*, 33(47):8351.

Goswami, A., Chatterjee, M., and Mukherjee, S. (2022). Steady states and phase transitions in heterogeneous asymmetric exclusion processes. *Journal of Statistical Mechanics: Theory and Experiment*, 2022(12):123209.

Henkel, M. and Schutz, G. (1988). Finite-lattice extrapolation algorithms. *Journal of Physics A: Mathematical and General*, 21(11):2617.

Pelizzola, A. and Pretti, M. (2017). Cluster approximations for the tasep: stationary state and dynamical transition. *The European Physical Journal B*, 90(10):183.